THESIS FOR THE DEGREE OF DOCTOR OF PHILOSOPHY

Solid Foams from Cellulose

Eliott Orzan

Department of Chemistry and Chemical Engineering
Division of Applied Chemistry
Chalmers University of Technology
Gothenburg, Sweden, 2025

Solid Foams from Cellulose

Eliott Orzan

Doktorsavhandlingar vid Chalmers tekniska högskola
Ny serie: 5676
ISSN 0346-718X
ISBN 978-91-8103-218-5

Department of Chemistry and Chemical Engineering
Chalmers University of Technology
SE-412 96 Gothenburg, Sweden
Phone: +46 (0)31 772 1000
www.chalmers.se

Cover image: A tree rebuilt from cellulose fiber foams which were produced over the course of the PhD work.

Printed by Chalmers Digitaltryck
Gothenburg, Sweden, May 2025

Solid Foams from Cellulose

Eliott Orzan
Chemistry and Chemical Engineering
Chalmers University of Technology

Abstract

The development of lightweight materials such as foams highlights the human drive to optimize material functionality and minimize energy expenditure. At the forefront of modern foam materials are highly versatile fossil fuel-based plastics; a technological triumph which is producing a spiraling ecological disaster. To solve this problem, we can turn to renewable materials such as cellulose. However, several challenges appear when transitioning to these materials: Solid foams from cellulose can suffer from lackluster mechanical performance, sensitivity to environmental conditions such as moisture and fire, and require significant energy to dry. This thesis explores structural features in cellulose foams which introduce multi-functionality such as enhanced mechanical strength and fire-retardancy.

Two distinct phenomena affecting the strength of cellulose networks were evaluated: i) degradation/cross-linking, and ii) structural rearrangement. The degradation of non-crystalline cellulose fiber regions weakened fiber networks via phytic acid or endo-xylanase enzymatic hydrolysis. To counteract this, fibers were cross-linked through the physical adsorption of extrinsic xylan or by covalently binding phytic acid to cellulose via dehydration synthesis reactions. Phytic acid also changed the foaming behaviour of wet systems applying an ionic surfactant, and imparted thermal stability and fire-retardancy to dried cellulose fibers. The structural arrangement of cellulose nanocrystals in suspensions and during freezing was modified by leveraging interactions between tert-butanol and water. The disrupted assembly and unique ice crystal formation led to tailorable strength and surface areas in freeze-dried cryogels.

With these studies, we unveil methods and mechanisms to strengthen fiber networks with the goal of expanding the use-cases of cellulose foams. In our pursuit of a sustainable future, we must overcome our dependence on non-renewable plastics by finding and exploiting effective solutions found in nature.

Keywords: Natural fibers, cellular solids, porous, aerogel, biopolymer

List of Publications

This thesis is based on the following appended papers and manuscripts:

Paper I:

Elucidation of cellulose phosphorylation with phytic acid
Eliott Orzan, Aitor Barrio, Stefan Spirk and Tiina Nypelö
Industrial Crops and Products, 2024, 218, 118858.

Paper II:

Foaming and cross-linking of cellulose fibers using phytic acid
Eliott Orzan, Aitor Barrio, Veronika Biegler, Jana Schaubeder, Alexander Bismarck, Stefan Spirk and Tiina Nypelö
Carbohydrate Polymers, 2025, 347, 122617.

Paper III:

Tert-butanol as a structuring agent for cellulose nanocrystal fluids and foams
Saül Llàcer Navarro, Eliott Orzan, Ratchawit Janewithayapun, Paavo Penttilä, John Andersson, Anna Ström, Roland Kádár and Tiina Nypelö
Accepted for publication in Biomacromolecules.

Paper IV:

Role of intrinsic and extrinsic xylan in softwood kraft pulp fiber networks
Jana B. Schaubeder, Stefan Spirk, Lukas Fliri, Eliott Orzan, Veronika Biegler, Chonnipa Palasingh, Julian Selinger, Adelheid Bakhshi, Wolfgang Bauer, Ulrich Hirn, and Tiina Nypelö
Carbohydrate Polymers, 2024, 323, 121371.

Contribution report

Paper I:
Main author. Designed experiments and prepared all samples. Wrote the first draft, edited, and reviewed the manuscript. Performed all measurements and analysis except measurement of NMR and elemental analysis.

Paper II:
Main author. Designed experiments and prepared all samples. Wrote the first draft, edited, and reviewed the manuscript. Performed all measurements and analysis except measurement of cone calorimetry.

Paper III:
Shared main author. Co-wrote the first draft, edited, and reviewed the manuscript. Performed freeze-drying of CNC suspensions, SEM and density/porosity measurements. Participated in analysis of WAXS, SAXS, rheology, surface area, and compression testing.

Paper IV:
Co-author. Performed HPAEC sample preparation, experiments and analysis. Edited and reviewed the manuscript.

Papers not included in this thesis

Xylan-cellulose thin film platform for assessing xylanase activity
Jana Schaubeder, Jonas Ravn, Eliott Orzan, João Manfrão-Netto, Cecilia Geijer, Tiina Nypelö and Stefan Spirk
Carbohydrate Polymers, 2022, 294, 119737.

Cellulose modified to host functionalities via facile cation exchange approach
Panagiotis Spiliopoulos, Saül Llàcer Navarro, Eliott Orzan, Reza Ghanbari, Rudolf Pietschnig, Clemens Stilianu, Stefan Spirk, Andreas Schaefer, Roland Kádár and Tiina Nypelö
Carbohydrate Polymers, 2024, 332, 121857.

Acknowledgements

It gives me great pleasure to acknowledge the people who made this journey not only possible, but also enjoyable. This has been an unforgettable arc in my life. Whether times were calm or tumultuous, inspired or drab, this time was marked by the people who I am thankful were part of it all. I have many words to say to many people but to sum it up, thank you all!

The BreadCell project which envelopes my PhD was funded by the EU under the H2020 Research and Innovation Programme (grant agreement No 964430). I am grateful for the opportunity to contribute to such an exciting and impactful project. The incredible collaborations and discussions were only possible from this funding. Tiina, as our fearless leader during the project, and my supervisor for this PhD, I want to thank you most of all. The combination of vision, organization, dedication, and fun-loving spirit was what made this experience. Thank you for guiding me back on track when my thoughts went on off-roading adventures. You're a real inspiration and I look forward to working together again! Thank you to my co-supervisor Cecilia for the fantastic discussions and guidance. Even though our fields felt distant for both of us at times, you inspired a sense of wonder in me for the world of microbiology. I also want to thank the good folk of the BreadCell project, Wolfgang, Alex, John, Georg, Florian, Clemens, Sonia, Olatz, Aitor, Ainhoa, Maialen, Ingemar, Terepsi, and Susanne. Special thanks to my fellow PhDs Jana, Markus, and Nesrine for the memorable times we spent outside work. And finally to my FOAMO co-founders Stef and Veronika: Stef your passion for life and work has really set a fire in all of us. And Veronika, my friend turned colleague turned business partner, what a crazy rollercoaster we've been on!

I would like to thank my examiner Hanna Härelind for the guidance and trust throughout my PhD work. A special thanks also goes out to Anna Ström, Romain Bordes, Nina Kann and Anette Larsson for the support and great discussions making my time at Chalmers smoother and more interesting! A final thanks goes to Fang Liu and the LIGHTer PhD network, an amazing opportunity for networking and scientific discussions on lightweight materials.

My daily life would have been colorless without my office mates. I realize now that I looked forward to being in the office knowing that you would be there.

Saul, we've had our laughs, our chats, our shared frustrations, and ultimately we finally published the paper, cheers to you. To Eva, and I guess Monika and Giovanni too? The late nights and chaos shared with you three will always be special memories. And to the rest of the PhD crew at Chalmers, Nikole, Guido, Jakob, Giannis, Jesper, Maja, Alex, and Maria, I appreciate you all for always being good company.

Now to my oldest friends in Sweden, I'm so happy I got lucky to have met all of you soon after moving here. The shared hobbies, interests and memes made every moment out of work so enjoyable. Viktor, from games to vacation to co-hosting Thanksgiving and everything in between, life here wouldn't have happened the same without you and I truly appreciate that. Leo, we had the chillest moments and the most intense scientific discussions, and for that I'm glad we took the Chalmers adventure together. Christian, your puns are bad and your putting is worse, but at least you have good taste and I'm constantly laughing when you're around. Anton, aka the mountain man, your intense passion for life and games have always made for the most interesting conversations, god bless. Lena, always a bright point in any day, your excitement for adventures and a good time is infectious. To Amr and Timo, for our good talks and even better nights. Finally to Ale, Anna, Pierluigi, Chiara, Erik, Camilla, Maria and Clarissa, for the shared times together beyond count. I am honored to have people like you around who inspire and challenge me. A special thanks also goes out to my friends back home Hubert, Randy, Jordan, Vishnu, Vishal and Natalie!

Lastly and most importantly, to my parents. Who knows where I would have ended up without your love and guidance. I may have never met these amazing people or had any of these experiences without you always being there for me. From the beginning to every moment up to when I typed these words, I appreciate all of it and I love you both.

Eliott, May 2025, Göteborg, Sweden

Acronyms

BSKP:	Bleached softwood kraft pulp
BHKP:	Bleached hardwood kraft pulp
SDS:	Sodium dodecyl sulfate
CMC:	Carboxymethyl cellulose
PA:	Phytic acid
CA:	Citric acid
CNC:	Cellulose nanocrystals
CNF:	Cellulose nanofibers
TBA:	Tert-butanol
OH:	Hydroxyl group
FTIR:	Fourier-transform infrared spectroscopy
NMR:	Nuclear magnetic resonance spectroscopy
SAXS:	Small-angle x-ray spectroscopy
SEM:	Scanning electron microscopy
TGA:	Thermogravimetric analysis
SSA:	Specific surface area

Contents

CHAPTER 1

Introduction

To fully appreciate the presented thesis, it is the chef's recommendation to compliment your reading experience with a freshly poured beer and a slice of buttered toast. Cheers! These accompaniments hold the secrets to unraveling the world of foams. Take a moment to notice the bubbles that form at the bottom of the glass and travel upward to develop the head of the beer; How do they form and why does the head shrink over time? A bite of crispy bread reveals that the structure of the slice has changed during toasting: It is noticeably stiffer, and the pores have changed shape and size. These phenomena underline the concepts covered in this thesis and highlight the diversity in what we call foams. To begin our exploration, we can turn back to nature as the original inspiration for our interest and need to study solid foams.

Consider a toucan. Like any living organism, it needs energy to sustain itself. However, it has a beak that is large for its body size. The apparent weight of such a large beak would require a significant expenditure of energy if the bird were flying. Within lies the secret: a network of keratin struts surrounding large pockets of air (Figure 1.1). The cellular structure is incredibly lightweight, and yet the toucan's beak maintains functional strength. This represents a class of materials known as foams, which are defined by their low mass to volume ratio, or density. The toucan's beak weighs just one-thirtieth of the bird's total mass while occupying one-third of its size, having a density of only 100 kilograms per cubic meter.[1,2] The structure is light enough to fly with and provides a unique evolutionary advantage for picking fruit up high or defending a nest. Herein lies the purpose and importance of foams. These cellular solids, proven by nature to optimize function to weight, are now inspiring the next generation of materials engineered by humans.[3]

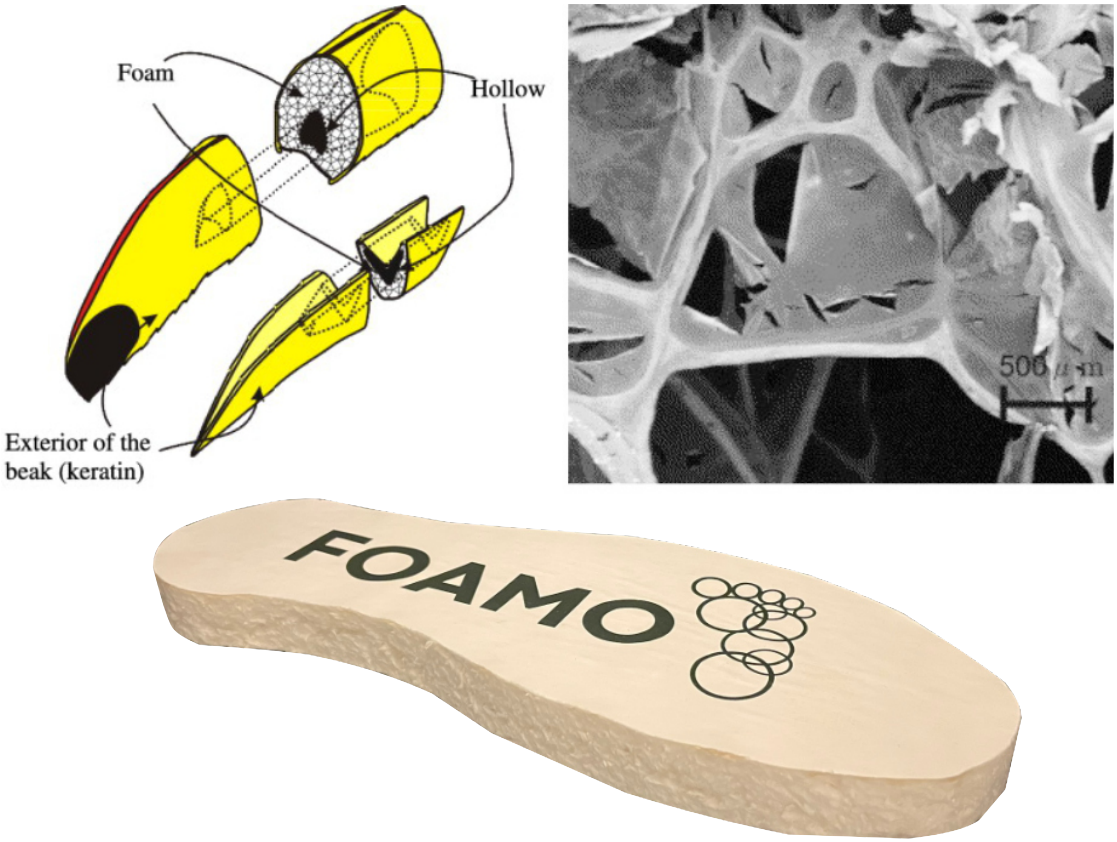

Figure 1.1: Cellular solids within a toucan's beak and applied conceptually to a shoe midsole. Reproduced from Seki et al.[2,4] Elsevier license: 6001330114791.

Many of the tools and products developed early in the course of human civilization were created to solve problems, perform tasks, and provide an improved standard of living. We prioritized functionality using any material, in any quantity, using any process. However, as our population grew, we became increasingly dependent on both materials and energy. Foams provide an elegant solution to this growing need. We can maintain function while minimizing material costs, leading to reduced energy expenditures in both processing and transportation. Globally, the packaging, automotive, and construction sectors represent the largest consumers of raw materials. Each of these industries has since adopted foams as critical engineering solutions.[5,6] Yet, in solving our problem of materials and energy, we inadvertently created another, an over-reliance on non-renewable fossil fuels.

We have long relied on fossil fuels (petroleum, coal, and natural gas) as an efficient source of both materials and energy. Plastics derived from petroleum are truly revolutionary in the context of human development, having become ubiquitous in the everyday products that we use. However, synthetic plastics, and by proxy, fossil fuels, are a non-renewable resource and thus finite. We have also discovered their unfortunate impact on global warming and the environment through the release and accumulation of greenhouse gases and microplastics.[7] We stand at a critical point where our hunger for materials and energy requires solutions to i) reduce the use and waste of fossil-fuel based materials and/or ii) find complementary renewable alternatives with competitive performance. Today, the complete replacement of plastics is a formidable, generation-spanning task. To transform our society into a true circular bioeconomy, we must develop solutions which are not only economically and technologically viable but also environmentally neutral. Polysaccharides such as cellulose may be a key component.

Cellulose represents the most abundant class of polysaccharides on earth and is found mainly in the cell walls of plant biomass. Since its discovery in the mid 1800s, cellulose has been implemented in numerous industrial sectors such as textiles, packaging, insulation, food, and paper products. The production, extraction, modification, and application of cellulose remain prominent topics in academia by virtue of its renewable and abundant nature. Cellulose has found particular value within the foam market in packaging and insulation. However, it faces challenges due to sensitivities to moisture and inadequate mechanical strength for high-performance applications. The aim of this thesis is to explore and evaluate methods to strengthen cellulose fiber networks in an effort to expand their potential use-cases.

Purpose and Objectives

The thesis and PhD work presented here were performed under the Horizon EU funded project BreadCell (grant agreement No. 964430). In 2021, the project set out to develop a lightweight sustainable solution for the sports and transportation sectors; with overarching themes of sustainable mobility, safety, and resource efficiency. Wood pulp fibers were transformed into high-value foam materials with an emphasis on process scalability and product safety. However, foam materials from wood pulp fibers were traditionally unsuitable for these applications and displayed significant barriers to entry.

Herein lies the challenge set for this PhD: develop a strong yet lightweight foam from wood pulp fibers and other renewable materials using a novel foaming technology. Material and energy efficiency, as well as scalability, were designated critical parameters to consider during foam development. The project was successful in achieving its goals of foam production (Figure 1.2); preventing a detailed discussion of the nature or results of the foaming technology in this thesis. However, several important questions emerged over the course of the project that generated the ideas presented here.

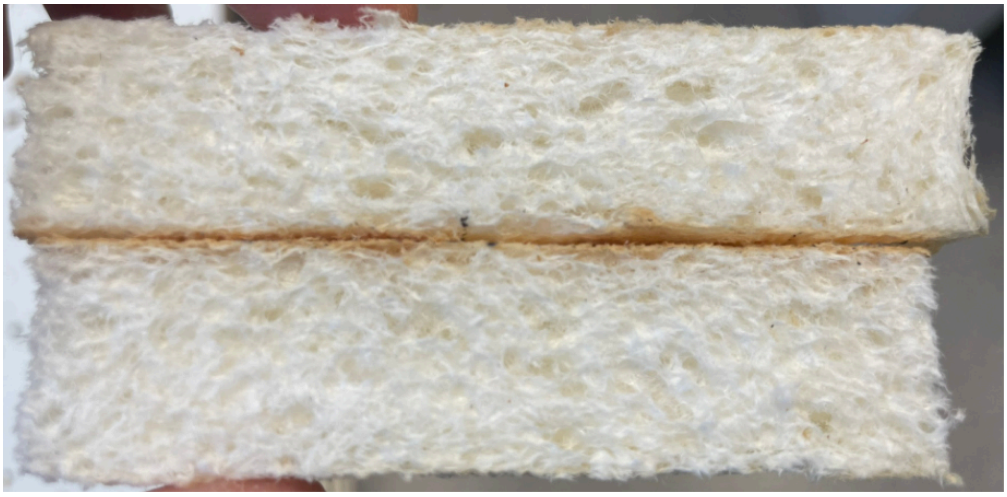

Figure 1.2: Cellulose fiber foam produced from the work in this PhD project.

In this thesis, I demonstrate methods to produce and strengthen cellulose foams. The underlying principles governing fiber network strength are explored through i) the degradation / cross-linking of cellulose fibers and ii) structural rearrangement. These investigations also produced multi functionality in the form of fire-retardancy and surface area. Moreover, this work seeks to answer the question of how wet foams can be formed and stabilized, similarly to how bubbles in beer and bread are made. Several drying methods are then presented and applied in an effort to create solid foams which are stronger and stiffer, just like toasted bread.

In **Paper I**, the covalent cross-linking of cellulose fibers with phytic acid (PA) was investigated. The phosphate groups present in PA provided additional value as a flame-retarding agent. Analysis of condensation reactions and fiber structure provided the foundation for the foams developed in Paper II.

In **Paper II**, the formation and performance of PA cross-linked cellulose fiber foams was evaluated. The effect of PA on foaming, compressive behavior and fire-retardancy showcased the unique benefits of this strengthening agent.

In **Paper III**, tert-Butanol was used as a structuring agent for cellulose nanocrystal suspensions and freeze-dried foams. Where all other publications employed oven-drying methods, here, liquid nitrogen and freeze-drying were used to create solid foams. Tert-butanol rearranged the physical configuration of CNCs in solid foams, changing the resulting strength and surface area.

In **Paper IV**, the effect of xylan in fiber networks was evaluated. This hemicellulose native to the structure of cellulose fibers was degraded from wood pulp fibers or added extrinsically through adsorption.

CHAPTER 2

Background and Theory

The following chapter breaks down the fundamental concepts underlying the results presented in the appended papers and this thesis. First, basic foam terminology is defined and the physics of foam formation and stability are established. Next is a summary of the chemical and structural composition of cellulose, as well the introduction of phytic acid (PA) as an additive. Finally, the effect of pores and fibers on the compressive behaviour of cellulose fiber solid foams is discussed. This chapter contains modified excerpts from my licentiate thesis work.[8]

2.1 The World of Foams

Foams are defined as gas bubbles dispersed in a liquid or solid phase. For the purposes of this thesis, a wet foam is a gas phase encapsulated by a liquid solution or suspension, and solid foams are dried solid materials enclosing gaseous spaces. The gas phases form cells or pores, and the extent to which they are surrounded by solid material determines the properties and application of a foam. When a cell is completely encapsulated by the solid, it is considered a dispersed phase and forms a closed-cell morphology (Figure 2.1).[9,10] These foams are ideal for applications requiring strength in mechanical compression and thermal insulation and can best be exemplified by materials such as cork, building insulation, and buoyant pool noodles. When cells are instead connected to each other, forming a continuous gaseous phase, it is considered an open-cell morphology. These foams generate the lightweight and energy-absorbing characteristics of toucan beaks, sponges, and cushions (Figure 1.1 and 2.1). The foams developed in this thesis are made from cellulose fibers, which form open-cell morphologies due to the disparate nature of fibers.

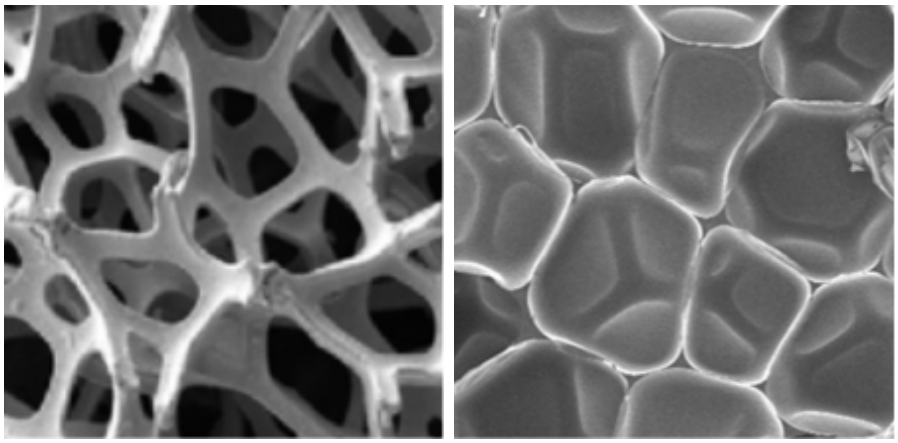

Figure 2.1: Representative images of open-cell and closed-cell foam morphologies. Reproduced from Brondi et al.[11] and Tolganbek et al.[12] under Creative Commons CC-BY license.

As material is added to a foam matrix, pore spaces within foams shrink and the walls surrounding pores thicken. This leads to an increase in density; defined as the mass of the material over its total occupying volume ($\rho = \frac{kg}{m^3}$). The potential for variation in foam structure therefore leads to a large distribution of properties (e.g. density, strength, thermal conductivity) that can fulfill a range of criteria. This can be visualized in an Ashby plot (Figure 2.2).[13] The

seminal works of Lorna Gibson and Michael Ashby guide our understanding of how material and cellular design influence foam properties.[9] They introduced the concept of relative density as a defining feature of foams, where the foam density ρ is divided by the intrinsic (or skeletal) density (ρ_s) of the solid phase materials. We can then divide material properties by their density to get the specific property value. This contextualizes how the materials and the structure affect performance and allows us to tailor lightweight materials for certain intended uses.

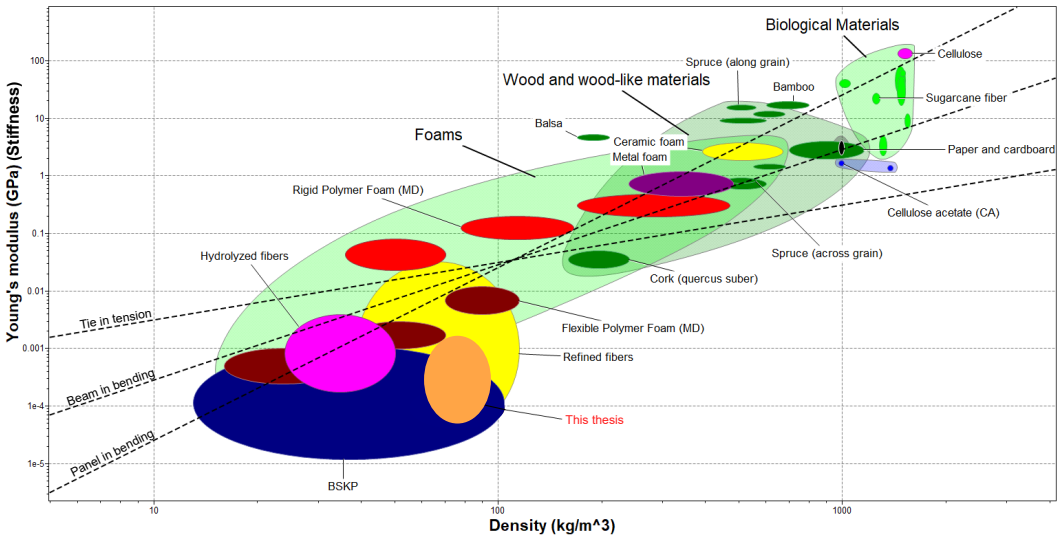

Figure 2.2: Ashby plot of common foams and cellulose-based materials created in Ansys Granta EduPack.

Solid foams can be made from nearly any material such as plastics, metals and ceramics. However, pressures placed on the environment due to the growing demand for non-renewable foam materials such as EPS or PU plastics require bio-based solutions which have competitive performance. Foams made from cellulose fibers have potential in this regard, having already been employed in packaging, absorption, and insulation solutions due to the inherent properties of the material and their open-cell morphology. Cellulose fiber networks have low intrinsic density and are loosly bound together. This allows for a lightweight construction that is capable of easily deforming to high strains; perfect for impact absorption in packaging. Fibers are also naturally non-conducting and thermally stable when transporting medical or electronic devices in warm conditions.[14]

2.2 Wet-State Foaming and Stability

The principle ways to introduce gas into a liquid are through i) dispersion, ii) condensation, and iii) templating methods. Dispersion methods involve the incorporation of the gas phase directly into the liquid media. This can be done by physical shaking/whipping (as in Paper II), sparging (bubbling gas up through tube/sieve), or pouring.[10,15–17] Generally, the homogeneity of dispersion foams is poor and they require additional stirring or the use of a sieve to control bubble size. Condensation methods instead rely on the gas phase being present as a saturated solute in the liquid. The gas phase is then released at nucleation points under energetically favorable conditions via boiling, cavitation (lowering pressure via movement), desorption, or reaction/decomposition.[10,15] Heterogeneous nucleation of gas pockets begins at interfaces while spontaneous nucleation occurs when $P > P_0 + (2\gamma/R)$, where P is pressure, γ is surface tension and R is the radius of curvature.[10] Finally, templating methods employ a removable liquid or solid phase to produce a porous structure. Recent studies have used oil-in-water emulsions, removable wax or starch scaffolds, polymeric particles, and ice as effective templating methods.[18–21] The shape and size of bubbles are strongly influenced by forces acting on them. Hydrostatic pressures affect size, while viscous traction alters the shape of rising bubbles. In larger bubbles, the latter effect is more pronounced as bubbles tend to elongate perpendicular to gravity.

Regardless of the foaming method, wet-state foams are thermodynamically unstable. Pore structures gradually change shape and collapse over time as a result of pressure-driven liquid and gas diffusion. We can understand these phenomena through the Young-Laplace equation for capillary pressure ΔP at gas-liquid interfaces (Equation 2.1):

$$\Delta P = \gamma\left(\frac{1}{R_1} + \frac{1}{R_2}\right) \tag{2.1}$$

Surface tension γ represents the energy difference between molecules at the surface and in the bulk solution (surface energy per unit area). Energy is therefore required to extend or form new surface area. As the total Gibbs free energy of a system will drive towards lower energy, foams will gradually minimize their total surface area over time, leading to instability.[22]

The main processes causing foam instability are: i) drainage/evaporation, ii) coalescence, and iii) coarsening (Figure 2.3).[23–25] Drainage and evaporation represent the removal of water from the lamellae between bubbles. As liquid drains due to gravitational forces, bubbles approach, forming thin films and plateau borders (Figure 2.4). Plateau borders are the nodes between bubbles, which possess lower capillary pressures and higher concentrations of solutes compared to the films. The pressure difference engages capillary flow to plateau borders which thins the lamellae. Eventually, the film ruptures and the bubbles coalesce.[10] Simultaneously, differences in capillary pressure between bubbles of various sizes cause diffusion of gas molecules (Equation 2.1).[23,26] This leads to the gradual disappearance of small bubbles as they feed into larger bubbles, known as coarsening or Ostwald ripening. The relative change in surface area and the reduction in curvature are energetically favorable.

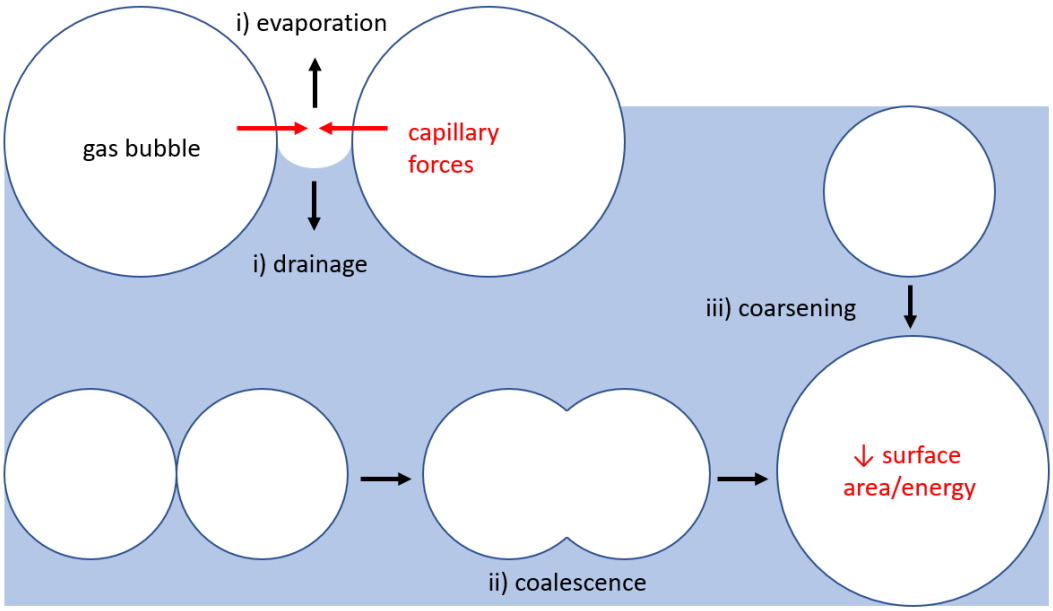

Figure 2.3: Foam destabilization mechanisms.

Surfactants, polymers and particles are used to prolong the stability of foams by increasing repulsive forces between surfaces, known as disjoining pressure.[16] Surfactants such as sodium dodecyl sulfate (SDS) are surface-active molecules that adsorb at gas-liquid interfaces, decreasing surface tension.[22] As capillary flow evacuates lamellar regions toward Plateau borders, the Marangoni effect opposes the flow as a gradient in surface tension sends surfactant molecules

to lamellae (Figure 2.4). Surfactants are thus used when foaming and help stabilize gas-liquid interfaces. They reduce drainage rates and coarsening by reducing surface tension, inducing shear viscosity, and providing resistance to gas transfer through the addition of lamellar mass.[23,24,26] Coalescence is also delayed due to the increased disjoining pressure from electrostatic and steric effects. Polymers such as carboxymethyl cellulose (CMC) are used to generate viscous and electrostatic effects in the lamellae, promoting stabilization effects. Particles can generate similar effects in the form of Pickering emulsions, stabilizing gas bubbles to form homogenous pore morphologies.[27–30]

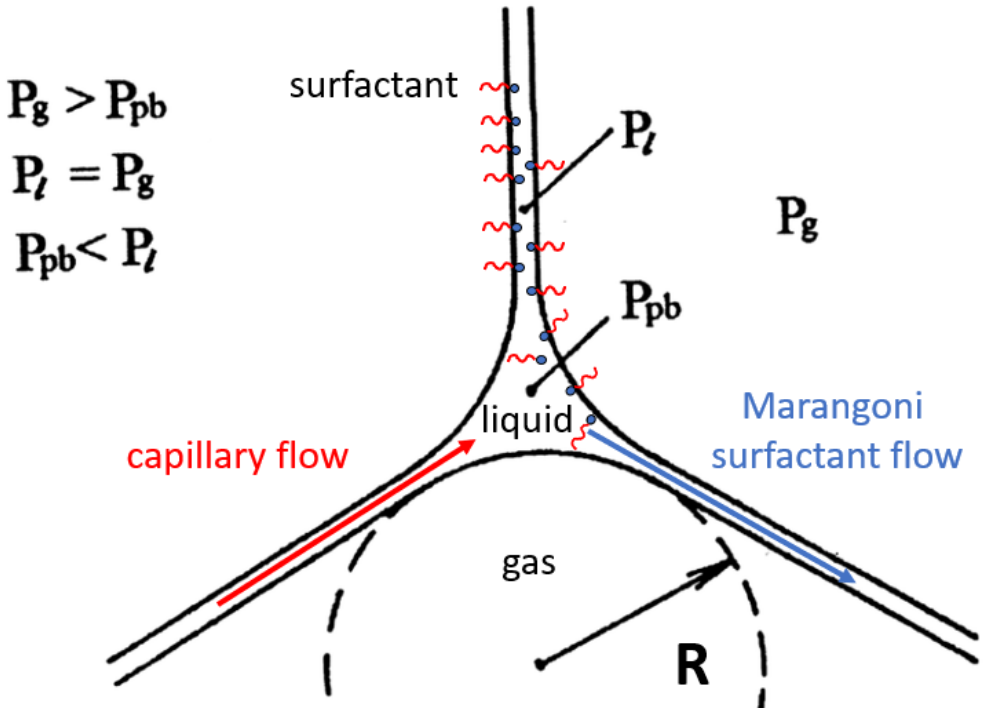

Figure 2.4: Material flows in Plateau border and lamellae. Reproduced and altered from Bikerman[10] Springer Nature license: 6015270938766.

In this thesis, CMC and the ionic surfactant SDS are employed as foam forming and stabilizing agents. A whipping dispersion method is used to create foams with cellulose fibers and the effect of phytic acid (PA) on the foaming behaviour of CMC-SDS solutions is analyzed.

2.3 Drying Techniques

Transformation of wet foams and hydrogels to lightweight, dimensionally stable porous materials requires the removal of the liquid phase. Drying converts liquids within the continuous phase into a gas that is then completely removed from the substrate. Drying is a great challenge in many industries (foams, food, pharmaceutical etc.) as it requires balancing of energy expenditure, time, scalability, and structural changes. In this section, the fundamental aspects that govern structural stability during drying will shed light on the advantages and disadvantages of modern drying processes. Evaporative and freeze drying will be mainly covered, with a brief discussion of alternative methods (supercritical CO_2, superheated steam) and supplementary techniques (electromagnetic radiation, ultrasound).

The terminology used to define dried lightweight materials is contentious and often does not obey strict guidelines. The most commonly applied terms, aerogel and foam, can be found interchangeably depending on the context of the study. This emerged as a result of two related methods for classification: one based on the pore structure (porosity, surface area, pore size) and one based on the drying process (evaporation, sublimation, supercritical). Aerogels were originally defined by Kistler in 1931 as having extremely low density (< 0.2 g/cm^3), high porosity ($> 90\%$), and meso-pore sizes (2 - 50 nm). Foams instead broadly encompass porosities over 50% and pore sizes over 50 nm.[31,32] However, advances in material and drying technologies have produced hierarchical structuring that blurred the lines between these definitions. In this thesis, classification is determined by the method of preparation and drying. The terms aerogel, cryogel and xerogel refer to the drying method while solid foams are used as an umbrella term for any dried solid-phase material with gas dispersed within (Figure 2.5a,b).

2.3.1 Evaporative Drying

The archetypal method for drying substrates applies air convection, heat, and/or pressure to change a liquid phase into a gas via evaporation. This process forms the basis for solid foams made from wood pulp fibers described in this thesis. Liquid molecules diffuse to a surface and, with sufficient heat and pressure, attain enough energy to reach their latent heat of vaporiza-

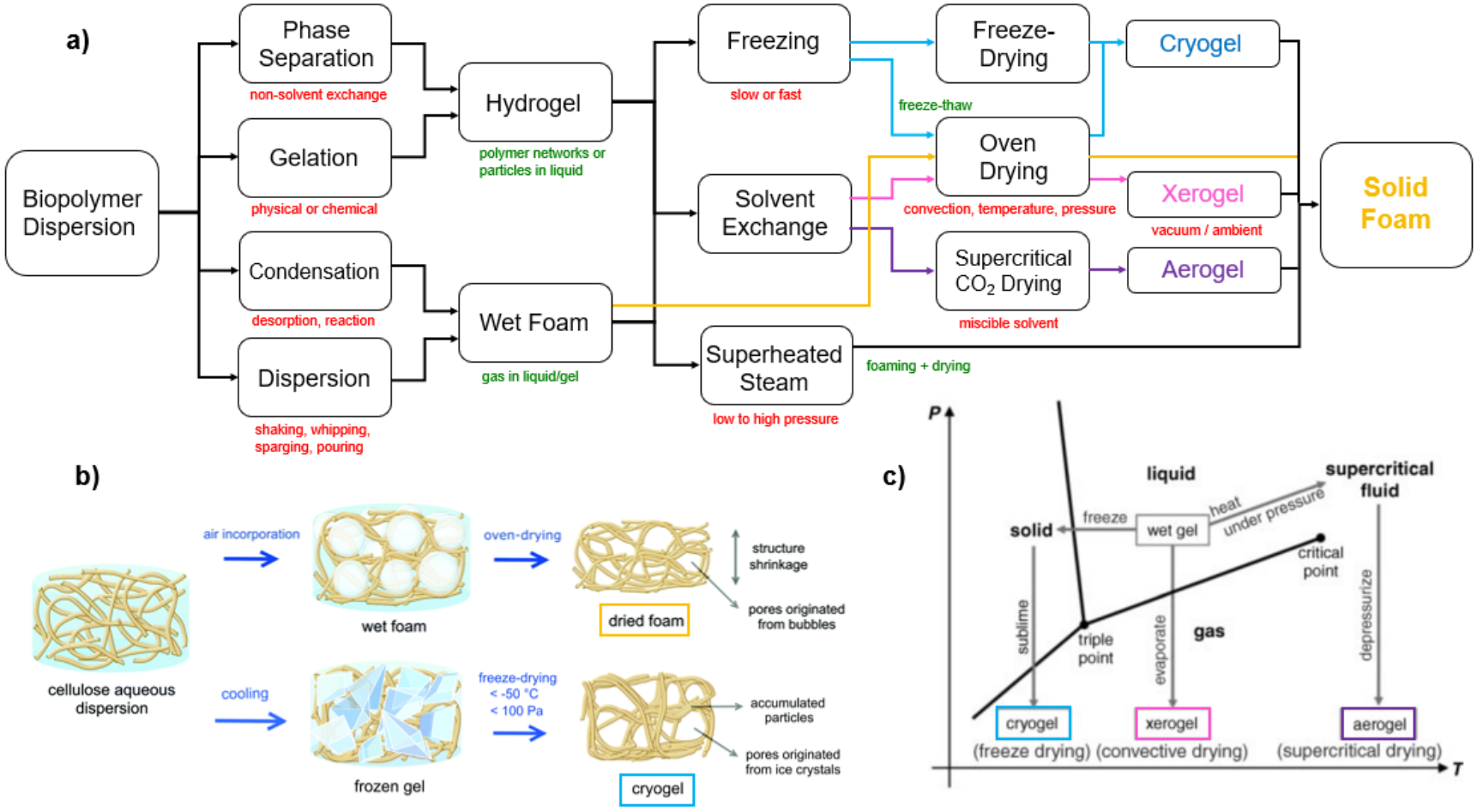

Figure 2.5: a) Flowchart of foam production. b) Schematic representation reproduced from Ferreira et al.[33] RSC license: 1603228-1 c) Phase diagram of water with drying method paths. Reproduced from Metzger et al.[34] Wiley license: 6015550621103.

tion and transform into the gaseous phase. The application of low-pressure vacuum can help in achieving this transition (Figure 2.5c).[35] The gradual accumulation of gas molecules in the bulk gaseous phase and in the Knudsen layer leads to an increase in vapor pressure, which thermodynamically limits evaporation. Thus, the introduction of air convection can accelerate the evaporation process.

Evaporative drying is the simplest and most scalable process, yet it suffers from issues of stability and energetic inefficiencies. First, evaporation occurring at gas/liquid interfaces leads to capillary pressures, resulting in converging surfaces and structural collapse. This change in structure represents the primary disadvantage of using evaporative drying, as maintaining dimensional stability in the face of capillary stresses is challenging. Second, heating of the substrate is typically dependent on convection through the impingement of hot air. The use of convection to heat a liquid or solid substrate is inefficient and leads to uneven heating and/or temperature gradients in thick substrates such as foams. High temperatures or exposure can also lead to undesirable color changes or material degradation.

The removal of water from a porous structure depends on the material and pore size. Larger macroscopic pores (> 50 nm) such as those found in the fiber foams in this thesis lead to faster drying rates due to fast diffusion and evaporation of water. However, rapid change in the structure and heterogeneity of these foams leads to shrinkage as internal stresses build up. Smaller pore sizes lower the diffusion and evaporation rates, leading to less cracking or deformation.[34] A hygroscopic material such as cellulose will contain free water and bound water molecules.[36] Bound water is adsorbed to sorption sites such as OH groups on cellulose fibers and requires energy to remove. Free water represents molecules in intercellular spaces that diffuse rapidly through a foam. The drying rate of a foam changes over time as water is removed. At a high moisture content, free water diffuses to surfaces, causing a plateau in drying rate. The removal of water leads to a reduction in volume and shrinkage at the surface, which in turn forms a densified skin layer. The formation of this dried layer on the outer surfaces of the foam, along with bound water, causes a reduction in the drying rate over time. The liquid pressure difference between the bulk and surface causes liquid to be pumped to the surface in accordance with Darcy's law. The migration of water through a matrix during drying is complicated yet can be described reasonably well by the Page model, derived from Fick's second law of diffusion.

Solvent exchange is a method which aims to preserve pre-existing porous structures during evaporative drying. This technique is often used to create xerogels or avoid the collapse of the lumen in never-dried cellulose fibers.[37] The water-containing foam or gel is submerged in a solvent such as hexane which has significantly lower surface tension and/or vapor pressure. This reduces the capillary forces which would cause shrinkage or collapse. However, the need for solvents (toxic or not) and the time needed for the slow diffusion restricts the applicability of this method.

2.3.2 Freeze-Drying

One method of circumventing the capillary forces which cause shrinkage and collapse in foams is via sublimation. The liquid within the material is frozen and the pressure is reduced under vacuum, granting a direct transition from solid to gas without formation of a liquid-vapor interface. This process can be referred to as freeze-casting or lyophilization, and forms what are known as cryogels. In this thesis, freeze-drying of cellulose nanocrystal (CNC) suspensions with tert-Butanol (TBA) as a co-solvent produced unique pore structures ascribed to the formation of ice crystals. Changing the freezing rate, direction, or solvents provides flexibility and control over the pore structure of the final foam/cryogel.

Lowering the temperature of liquids to below their freezing point causes the formation of ice crystals. A slow descent in temperature results in lower nucleation rates as it is thermodynamically favorable to grow existing ice crystals.[38,39] This inevitably produces larger ice crystals and thus larger pores. Rapid cooling of the system using for example liquid nitrogen, causes spontaneous nucleation over a multitude of locations. The growth of the ice crystals is then volumetrically limited, producing smaller crystals and smaller pores. As the ice crystals grow, solid-particles such as CNCs are pushed to the interstitial spaces, forming the pore walls. This process is known as ice-templating.[40] The orientation of pore walls can also be controlled by changing the thermal gradient in the mold. With uniform exposure throughout the system, ice crystals will presumably grow isotropically outward in all directions. By subjugating one side to lower temperatures, ice crystals will form in columns perpendicular to the exposed plane.[41] These anisotropic formations create capillary structures reminiscent of those found in wood.

The introduction of solvents can influence the growth of ice crystals and sublimation conditions. TBA is one such solvent that increases sublimation rates and limits the growth of ice crystals.[42–44] This is due to TBA and water are miscible and form eutectic mixtures at approximately 20 and 90 wt% addition of TBA.[45–47] Typically, two solvents will freeze mostly independently according to their individual melting/freezing points. However, at the eutectic composition only a single freezing point exists, which sits at a lower temperature than either TBA or water. TBA and water also form hydrogen-bonded liquid micro-clusters, limiting the growth of ice crystals.[48,49] This leads to a better preservation of the original wet-state network structure.[50] Outside of the eutectic mixture, TBA also influences pore structuring by forming needle-shaped dendritic crystals.

Freeze-drying represents a drying technology which has promise for industrial scalability. Currently, the food and pharmaceutical sectors employ this technology however, the energy and time demand required to freeze-dry materials is considerable.[51] The traditional batch-style operation was transformed in the 1960s to a continuous production which solved issues of heterogeneity. In addition, novel atmospheric freeze-drying has been investigated which circulates dry cold air to create a moisture gradient. This technology is more energy efficient yet sacrifices in the time demand.[52]

2.3.3 Supercritical and Superheated Drying

Supercritical drying involves the extraction of the liquid phase with a miscible compound at supercritical conditions. When supercritical, liquid and gas phases become indistinguishable and thus the issues related to surface tension and capillary forces become obsolete.[34] Upon isothermal depressurization, the pore fluids are removed from the material, leaving a dried porous material with an intact structure. This process produces high surface areas and small pore sizes, forming what are known as aerogels. Carbon dioxide has become the most industrially relevant compound for this application due to its low supercritical temperature and inertness. However, supercritical drying requires significant pressurization in enclosed chambers, leading to safety and scalability considerations. The energy and solvent needs also limit industrial viability. If the pore liquid is not miscible with carbon dioxide, other relevant solvents typically require significantly higher temperatures for supercriticality which can cause material deformation. In cellulose-based aerogels, a time-consuming

solvent exchange step with alcohol or acetone is necessary for the application of this drying process.

A relatively novel process developed in the food industry employs the use of superheated steam to dry materials.[52–54] Saturated steam is heated to form superheated steam in an enclosed chamber. Inside, the material heats up and evaporated moisture is picked up by the steam. The evaporation process is only reliant on heat transfer (no heat of vaporization) as there is little resistance to moisture diffusion into its own vapor. The process can be run anywhere from low to high pressure and must be run above the inversion temperature to have superior drying rates to hot air convection. The relatively high energy efficiency of this process lies in the reuse and recovery of heat. Energy savings of 50-80% were achievable, giving it potential industrial relevance.[55] It is also possible to condense and recover toxic or volatile components.[52,54] A unique aspect of the superheated steam process is the formation of porosity as elevated temperatures cause boiling and vaporization within the material.

2.3.4 Assistive Processes

Modern applications of evaporative and freeze drying techniques make use of electromagnetic radiation and ultrasound to aid in water removal.[34] These processes are commonly used in conjunction with traditional drying techniques to improve efficiency. They help the migration and diffusion of liquid molecules from the core of a matrix to surfaces. Ultrasound can be thought of as mechanical oscillations that produce compression and decompression of the matrix. As it passes through viscous media, it will dissipate energy and cause liquid flow. The compression and decompression can cause cavitation, creating vapor bubbles inside the matrix, and affecting porous structures and cellulose fibers. Drying processes which instead employ electromagnetic radiation turn to infrared or microwave frequencies. Infrared units heat materials via absorbed thermal energy. It allows for uniform heating, though only to shallow depths from the surface. Microwave radiation on the other hand, penetrates through the material producing uniform internal heating. The vapor pressure from excited water molecules promotes movement to surfaces and reduces the energy need for vaporization. However, the high capital costs and poor conversion of energy input to absorption are undesirable. Controlling material temperature can be challenging, producing hot spots.

2.4 Materials

2.4.1 Cellulose

The primary base structural unit of wood and other plants is cellulose, a polysaccharide chain of β-1,4-linked glucose units. Each glucose unit features three hydroxyl (OH) groups, making cellulose particularly hygroscopic and thus sensitive to humidity. On the other hand, the presence of OH moieties allows cellulose surfaces to be modified via e.g. acetylation, oxidation or esterification reactions.[56] Cellulose chains link together to form elementary microfibrils composed of crystalline and amorphous regions.[57] At this scale, cellulose nanocrystals (CNCs) and cellulose nanofibers (CNFs) can be defined (Figure 2.6).[58,59] CNCs are produced by harsh acid hydrolysis of cellulose chains, leading to the formation of short crystalline fibrils. CNFs are processed in milder conditions via enzymatic pre-treatment, oxidation and mechanical disintegration. This results in longer semi-crystalline fibrils. Elementary microfibrils bundle together surrounded by amorphous hemicelluloses and lignin to form fibers.[60,61] A hierarchical structuring begins as fibril bundles develop in complexity to form the primary cell wall of plants such as trees.

Cellulose fibers referred to in this work are wood pulp fibers of hardwood or softwood trees. To form pulp fibers, wood is processed via chemical, mechanical and semi-chemical pulping processes to remove bark, lignin, and other impurities.[62] The pulp fibers used in Papers II and IV have undergone a kraft process, which uses sodium hydroxide and sodium sulfide to break down wood. A bleaching process then removes all residual lignin using a variety of chemicals or processes (e.g. hydrogen peroxide). Kraft pulp fibers also contain hemicelluloses; polysaccharides with short, branched chains of different saccharide subunits. Xylans and mannans make up the majority of hemicelluloses in woods. In Paper IV, intrinsic xylan was enzymatically degraded from cellulose fibers or extrinsic xylan from beechwood was adsorbed. Intrinsic refers to xylan originally derived from the wood whereas extrinsic originates from outside the source material. The carboxymethyl cellulose (CMC) added in Paper II is rather a derivative of cellulose where some OH groups are replaced by carboxymethyl groups.

Cellulose derived from wood and plants is a widely-available renewable resource with well-established industrial suppliers. It has production rates over

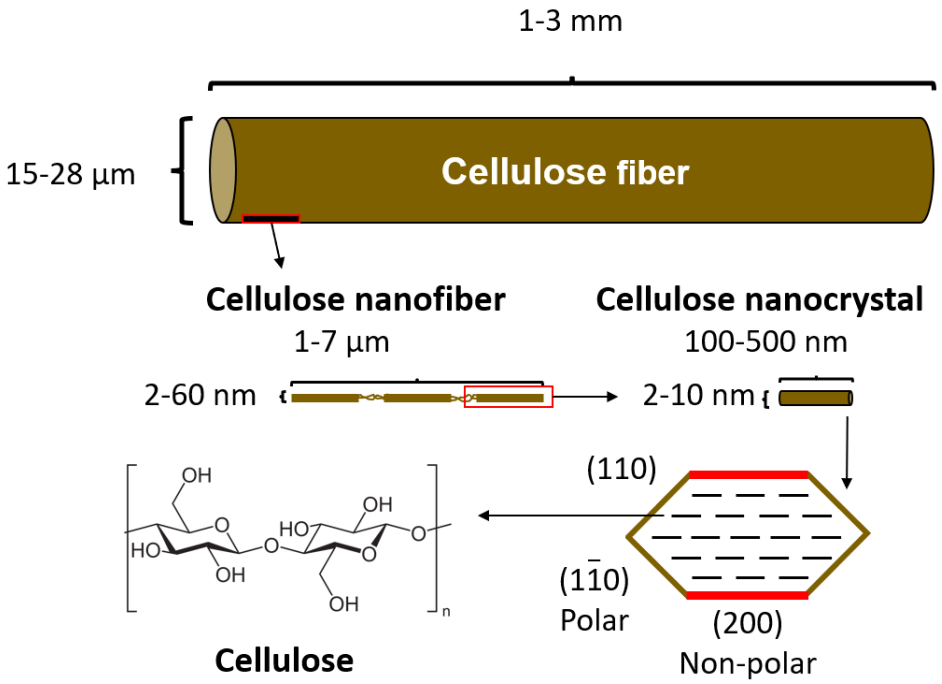

Figure 2.6: Schematic of cellulose fibers to nanocrystals structuring.

2 orders of magnitude higher than synthetic plastics putting it in a prime position for industrial-scale application.[63] CNCs and CNFs on the other hand are still challenged by the costs and capacity associated with their production. For now, their potential applications are in high-tech products such as optics, nanocomposites and biomedical, yet their limitations also prevent more wide-scale use. With CNCs, the largest drawbacks of their production process stems from the large quantities of dangerous chemicals needed, the poor reaction yield of CNC, and the high capital cost for equipment.[64,65] In addition, current alternative production routes to sulfuric acid hydrolysis have produced poor quality CNCs in scaled-up production and often lacked colloidal stability.[66] On the other hand, CNFs are not only expensive to produce, but also hard to characterize due to the mixture of CNFs and partially defibrillated fibers with a range of length scales.[67] To separate pulp into CNFs, mechanical grinding is applied which accounts for 10% of the manufacturing cost of the process. To reduce energy consumption, enzymatic and chemical pre-treatment of the pulp have been proposed to improve separation.[32,68] Acid or enzymatic hydrolysis, TEMPO-mediated oxidation or carboxymethylation create repulsive forces between fibers easing separation, however, the cost and waste generated from these processes is considerable.[64]

2.4.2 Phytic Acid

Also known as myo-inositol hexakisphosphate or IP6, phytic acid (PA) is extracted from the plant tissues of bran, seeds, and legumes. The unique phosphorylated structure has shown promise as an anti-oxidant in food, chelating agent for metal filtration, and anti-cancer aid in medicine.[69] Within the realm of celluloses, PA has been used in the production of nanocelluloses prehydrolysis treatment.[70,71] In this thesis, the multiple phosphate groups are used to cross-link bio-based materials and impart fire-retardancy.[72–76] Since the ban on brominated and chlorinated organohalogen flame retardants starting in 1977, considerable attention has been paid to renewable organophosphates such as phytic acid (PA) as suitable replacements.[77,78]

Phytic acid is soluble in water and thus requires cross-linking to remain on washable substrates.[73,75] A cross-link can be formed through condensation reactions of cellulose hydroxyl groups and phosphates. In Paper I, we explore the mechanisms which result in the formation of covalent diester bonds between these compounds. A common approach is to employ melamine or diacynamide.[74,79,80] This efficient reaction results in covalent bonding with improved fire-retardant properties due to the presence of phosphorus and nitrogen. However, amine catalysts are toxic and therefore studies have turned to urea and enzymes as alternatives.[74,76] It has also been suggested that weaker bonding through electrostatic interactions and hydrogen bonding may provide sufficient stability when formed via layer-by-layer deposition, yet substrate washability was not analyzed.[75,81]

We take a catalyst-free approach to cross-link phytic acid with cellulose fibers inspired by traditional fabric finishing techniques. There, citric acid is hot-pressed to fabrics imparting strength, wrinkle resistance and durability.[82] Hot-pressing at 120 - 180 °C allows condensation reactions via dehydration to form ester linkages between cellulose and citric acid.[83] This technique has also been applied to cellulose fiber foams as in Paper II.[84–87]

2.5 Fiber Foam Behaviour under Mechanical Compression

2.5.1 Compression Mechanics

As a foam is compressed, it undergoes three distinct deformation behaviours i) bending elasticity ii) buckling plateau and iii) densification (Figure 2.7). The linear elastic region at low strains (a) defines the modulus or stiffness of the material. In fiber foams, this is controlled by the resistance of the cell wall/fibers to bending. As more fibers are added to pore walls, the strength and stiffness of the foam increases, and the porosity goes down.[88,89] In closed-cell foams, gas is completely enclosed in material, which adds to compression modulus compared to open-cell foams.[9] In an open-cell configuration, walls are incomplete and thuscompression forces gas out of the pores. The material may retain some benefit if inter-pore connectivity is poor or high strain rates are used. The pore size also influences the density of fibers in the walls. Foams with large pores concentrate fibers in pore walls, increasing inter-fiber interactions. The thicker cell walls resist elastic deformation and can accomodate larger pores. However this also causes a decrease in yield stress with higher pore interconnectivity.[18,19]

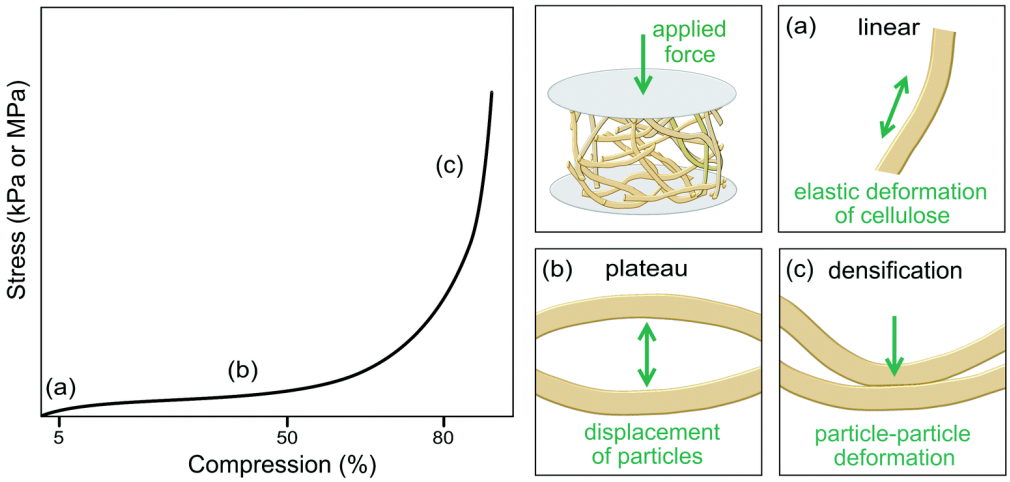

Figure 2.7: Stress-strain curve of foam material with regions a) linear elasticity, b) buckling plateau and c) densification. Reproduced from Ferreira et al.[33] RSC license: 1603228-1.

The second deformation region is known as the buckling plateau. At elevated stress levels, fibers begin to buckle, slip, displace, and ultimately fracture once the stress surpasses critical thresholds. Mechanical failure in fiber foams primarily results from weak inter-fiber bonds rather than failure of the fibers themselves.[27] Individual fibers will pull out and slip, dissipating energy in the process.[9] Consequently, the orientation of the fibers and the nature of their interactions dictate the overall deformation behavior of the material. Pöhler et al.[90] proposed that the foam's shape recovery is governed by the straightening of buckled fibers rather than the strength of fiber-fiber bonds. Recent studies have focused on modeling foam mechanics based on the deformation of individual fibers and fiber networks.[88–91] In the final stage of deformation, cell walls collapse completely and come into contact, leading to a steep rise in the stress-strain curve slope—marking the onset of densification.

In terms of energy absorption, a foamed material can be optimized to match application-based impact criteria while minimizing density. There is a critical point beyond which the cell walls undergo irreversible damage, no longer behaving as elastically buckling structures. In polymeric foams, this peak stress corresponds to the start of the densification region.[9] The area under the stress-strain curve up to this peak represents the maximum potential for energy absorption. For a foam to be reusable in impact-absorbing applications, it must absorb the full kinetic load without damaging its matrix. High-density foams may exceed the critical stress before sufficient energy is dissipated during the buckling phase, while low-density foams may collapse entirely before absorbing the required energy. Therefore, the optimal foam combines a plateau stress below the damage threshold with the ability to absorb all energy prior to reaching peak stress.[9,18]

Smaller pore sizes generally enhance compressive strength and structural uniformity in foams.[9,27] In contrast, wide pore size distributions introduce heterogeneities and structural irregularities, resulting in varied local deformation behavior. It is thought that the generation of larger pores in the matrix can be due to coarsening but also local opening of fiber networks during drying.[90] Under axial compression, the modulus, yield stress, and shear strength increase along the direction aligned with the longest dimension of the pore walls.[9,19] This directional strengthening often compromises mechanical performance along the perpendicular axis. Therefore, precise control over pore size and orientation is essential in selecting suitable applications for a given foam material.

2.5.2 Fiber Networks

Incorporating cellulose fibers into foam matrices introduces complexities absent in plastic and metallic foams. The fibrillar nature of cellulose inhibits the formation of closed-cell pores and leads to a strong dependence on fiber-fiber bonding for mechanical integrity. Long wood pulp fibers can bridge disconnected regions within the foam due to their length, but their coarseness often intensifies structural heterogeneity.[25] In contrast, CNCs and CNFs are significantly smaller, enabling short-range interactions that help distribute localized stresses more uniformly. However, CNCs and CNFs have lower individual mechanical strength than wood pulp fibers.[30,88] For optimal performance, hybrid networks combining the connectivity of CNCs/CNFs with the structural reinforcement of larger fibers can achieve both mechanical strength and network homogeneity, provided strong inter-fiber bonding is maintained.[27,30,40,88,90] Similar outcomes can also be achieved through fibrillation of pulp fibers or reintroducing fines, which reduces preprocessing demands.[90,92]

The mechanical properties of fiber foams are highly sensitive to fiber geometry, flexibility, bonding potential, and orientation. At low concentrations, fibers have fewer contact points and act more independently under load, resulting in non-uniform stress distributions and inconsistent mechanical response.[88,90] Increasing fiber density enhances inter-fiber contact and compressive strength, often following a power law relationship.[9,88,89] However cellulose fiber foams do not always follow the power-law exponent for open-celled structures proposed by Gibson and Ashby.[93,94] For foams similar relative densities, fiber packing and pore morphology in cell walls have been identified as key parameters governing mechanical performance.[19,27,88]

Due to their fibrous structure, wood pulp networks require physical entanglement or chemical cross-linking to prevent slippage under mechanical stress.[88,89] Surfactants like SDS are commonly used to stabilize foams and ensure uniform pore structures but can weaken fiber-fiber bonds through debonding effects.[27,90,92,95–97] To enhance bonding, conventional techniques involve hot-pressing of cross-linking agents such as citric acid or 1,2,3,4 - butanetetracarboxylic acid, which create covalent links between cellulose chains.[82,98] These covalent bonds replace weaker frictional interactions and improve network stability. In this work, phytic acid was used to cross-link cellulose, leveraging the reactivity of hydroxyl groups at the C2, C3, and C6 positions to reinforce the foam matrix.

CHAPTER 3

Materials, Methods, and Characterization

This chapter outlines the route by which all materials were selected, prepared, and characterized. First, descriptions and reasoning behind the preparation steps for all materials provides context to the development of the final substrates. Microanalysis of these substrates observes the phenomena impacting changes in cellulose structure, bonding and submicron arrangement. Finally, foam properties are investigated to how macro-scale behaviour and structure are influenced by the antecedent observations. All characterization techniques and results presented in this section were performed by or analyzed by the author and are central to the overall understanding of this thesis. Several methods utilized in the appended publications are not mentioned here to maintain relevancy to the subject matters in this thesis.

3.1 Substrate Preparation

Frothed fiber foams

The materials that form the cornerstone of this thesis are known as frothed fiber foams. The foams are composed primarily of bleached softwood kraft pulp (BSKP) fibers, with CMC and SDS acting as stabilizing agents. Mechanical agitation, otherwise known as frothing, introduces air into the fibrous network to create a more voluminous, lower-density structure. This methodology is well described in literature as a prominent way to create self-standing foam structures from natural fibers.[27,90,96,99,100] The work produced as part of the BreadCell project and this thesis has utilized these foams as a control group to understand chemical and structural modifications to fibrous networks in **Paper II**.

The first step is preparation of the foam components. Dried BSKP (85% spruce, 10% pine, 5% larch) was dispersed with a Noram disintegrator to a consistency of 4 wt% in distilled water and furthermore reduced to 14 wt%. 100% birch BHKP sheets were soaked overnight in distilled water, refined for 15 min (to 25°SR) in a valley beater according to ISO 5264-1 and reduced to a consistency of 14 wt%. CMC and SDS were dissolved in water to 2.5 wt% and 5 wt% w/w content respectively. Strengthening agents in **Paper II** include PA and CA, which were diluted to 5 wt% in distilled water.

To produce the foams, wood pulps were mixed together with strengthening agents using a hand-held mixer at a low speed setting. This action promoted dispersion of the strengthening agents throughout the fiber mixture while simultaneously breaking up clumps of wood pulp. To this mixture, CMC and SDS were added by mixing at low speeds until a homogeneous wet slurry was achieved as shown in Figure 3.1. Increasing the speed of the hand mixer to near maximum revolutions enabled the introduction of air into the slurry, which was captured and stabilized by CMC and SDS. Approximately 30 secs of frothing increased the volume by 25%, producing wet foams with volumes capable of filling a 10 x 10 x 2 cm Teflon mold. Particular attention was paid during mold filling to prevent the introduction of large interior air pockets or surface defects. Steel meshes were applied to the top and bottom during drying. These meshes allowed air flow and water evaporation across the surface of the wet foam while maintaining a smooth surface. All foams were dried at 80 °C in a 50% airflow convection oven for 12 hrs. This time was determined to be

the sufficient drying time to achieve a constant moisture content of 5 wt%. An overview of the final dry composition of all solid foams is presented in Table 3.1. The dried foams with PA and CA were then treated at 80, 120 and 160 °C for 180, 120, and 5 min respectively to allow condensation cross-linking reactions to occur between acids and cellulose; replicating conditions applied to similar materials.[72,82,84–87,98,101]

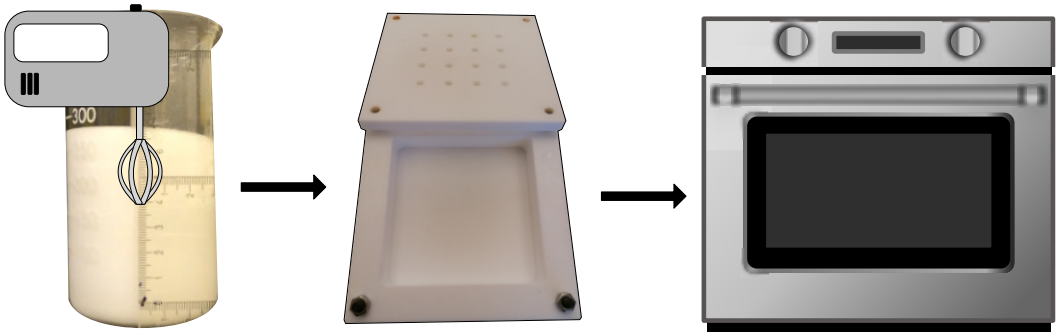

Figure 3.1: Frothed fiber foam forming process.

Table 3.1: Dry matter composition of solid foams produced in **Papers II, III, IV**. All foams except the CNC-TBA include approximately 5 wt% CMC and 0.7 wt% SDS and were dried at 80 °C for 12 hrs. When adding strengthening agents, the ratio between cellulose fibers, CMC and SDS were kept constant. a = P or C, whether phytic or citric acid was added. * = U or W, whether the cellulose filters were unwashed or washed after treatment.

Label	Cellulose	Strengthening agent (wt%)	Notes	Papers
BA*	70 wt% BSKP 24 wt% BHKP	-	blank control	I, II
a160*	67 wt% BSKP 23 wt% BHKP	5 wt% Phytic acid or 5 wt% Citric acid	reacted 160 °C for 5 mins	
a120*			reacted 120 °C for 120 mins	
a80*			reacted 80 °C for 180 mins	
xCNCyT	2-10 wt% CNCs	19-71 wt% TBA	Freeze-dried Figure 3.2	III

Phytic acid treated cellulose filters

In the course of investigating the properties that developed in the foams produced for **Paper II**, it became necessary to understand how PA affected the cellulosic microstructures. Therefore, in **Paper I**, pure cellulosic substrates in the form of filter papers (Whatman Cytiva qualitative filter paper, grade 5) were evenly coated with PA solution to replicate the exposure conditions of BSKP fibers in the foams. Using filters allowed an even and replicable coating of the acid across all fibers. The filters were then dried and heat treated in similar conditions to the foams. As a result of the reaction time and temperature, a number of products were anticipated alongside unreacted raw materials. Therefore, filters were subjected to a thorough washing step in order to remove any unreacted PA or PA molecules which had only bound to themselves. The filters were washed with 200 mL distilled water, 100 mL 95% ethanol, and again with 200 mL water until the water conductivity of the eluent no longer changed. Washed filters were once again dried at 80 °C for 1 hr and labelled with a W on the end while unwashed filters were given a U.

Cellulose nanocrystal suspensions and foams

In **Paper III**, CNCs were exposed to mixtures of TBA and water (Figure 3.2). The micro-scale interactions between water and TBA alter how CNCs arrange structurally within the suspensions. Therefore, varying concentrations of TBA were added to 10 wt% CNC suspensions while periodically shaking to avoid phase-separation. The suspensions were allowed to mix overnight to ensure a homogeneous distribution of all components. Suspensions were labeled xCNCyT where x and y represent the concentrations of CNCs and TBA in wt%, respectively.

To observe how interactions between CNCs, TBA and water in suspension affected the morphology of CNCs when transformed into a dry material, a freeze-drying methodology was employed. The CNC suspensions were set in thick-walled cylindrical molds and degassed before submerging completely in liquid nitrogen for several minutes. The frozen suspensions were freeze-dried at -105 °C for 2 days until completely dry. Liquid nitrogen was employed to ensure an near instantaneous freezing of the suspensions, guaranteeing increased nucleation zones for ice crystals. If subjected to higher temperatures or slower freezing conditions, larger ice-crystal would form and the resulting structure may have been more significantly affected by ice-templating.

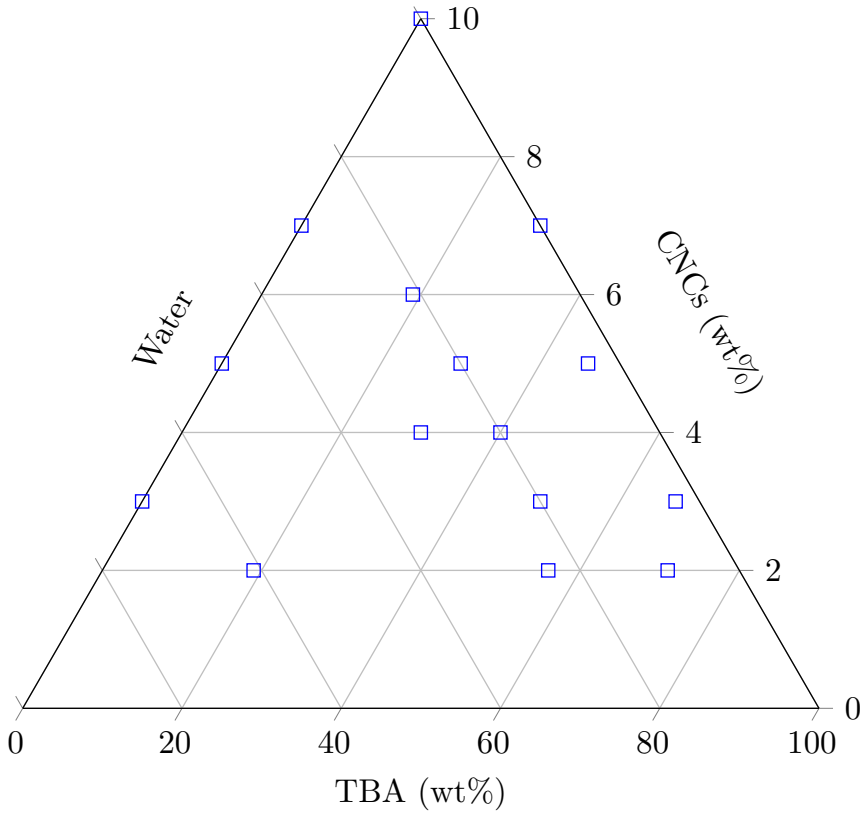

Figure 3.2: Ternary plot of CNC-TBA suspensions, where all compositions were chosen as part of a design of experiments in JMP software.

Xylan/xylanase treated hand sheets

The intrinsic strength bestowed on cellulosic structures by hemicelluloses was investigated in **Paper IV** by i) enzymatic degradation and ii) adsorption of xylan on cellulose fibers. BSKP was dispersed in water to 1.57 wt% consistency, refined in a valley beater for 45 min, and eventually formed into 80 g*m^{-2} hand sheets. Enzymatic degradation was carried out by introducing an endo-1,4-β-D-xylanase into the BSKP suspension at 50 °C and pH 6 for ideal enzymatic function. The suspension was slowly stirred before adding hydrogen peroxide to deactivate the enzyme. To contrast the degradative method, xylan adsorption was started by swelling and dissolving beechwood xylan in NaOH overnight before adding the BSKP suspension and adjusting the pH to 7. Blank samples were created by similar treatment of both degradation and adsorption methods without enzyme or xylan addition, respectively.

3.2 Sub-micron Molecular Analysis

FTIR and NMR of phytic acid treated filters

To investigate changes in the molecular structures and chemical environment of cellulose fibers treated with PA, a combination of fourier-transform infrared spectroscopy (FTIR) and nuclear magnetic resonance spectroscopy (NMR) techniques were performed.

FTIR spectroscopy is a technique based on the absorption of infrared radiation by molecules at specific wavelength. The absorbed energy creates characteristic rotational and vibrational energy gaps, forming a molecular fingerprint.[102] In **Paper I**, FTIR spectroscopy in the mid-infrared region (4000-400 cm^{-1}) was performed on the dried cellulose filters via attenuated total reflectance (FTIR-ATR). By correcting background noise and normalizing all spectra to intensity values at 4000 cm^{-1}, changes in bonding environment as a result of condensation reactions with phytic acid could be characterized.

NMR spectroscopy is a technique which observes transitions in the spin states of atomic nuclei when exposed to an external magnetic field.[103] The shift in response frequency provides information about the immediate chemical environment around specific nuclei. In **Paper I**, solid-state NMR was utilized, which tends to provide less precise spectra as anisotropic interactions cause a broadening of peaks. A 4mm ZrO2 MAS rotor recorded ^{13}C and ^{31}P NMR spectra, with detailed MAS rates and decoupling information provided in the appended manuscript. To understand peak and intensity shifts in the spectra, Gaussian deconvolution was performed. Via deconvolution of the ^{13}C NMR spectra, changes cellulose fiber crystallinity could be calculated:[104]

$$\text{Crystallinity } (\%) = \frac{A_{\text{crystalline}}}{A_{\text{crystalline}} + A_{\text{non-crystalline}}} * 100 \tag{3.1}$$

where A represents the area underneath the fitted Gaussian curves. The C4 carbon of cellulose produces distinct peaks for crystalline (89 ppm) and non-crystalline (85 ppm) moieties.

X-ray scattering of CNC-TBA suspensions

Small-angle X-ray scattering (SAXS) and wide-angle X-ray scattering (WAXS) are techniques which rely on the elastic scattering behaviour of x-rays from different incident angles to provide information on the structural organization of a material.[105] Depending on the angle, length scales from 1-50 nm can be probed to give information on particle and pore shapes and sizes, or distances in ordered materials. In **Paper III**, X-ray scattering of CNC-TBA suspensions was utilized to detect rearrangements in the micro-scale packing of CNCs as a result of solvent interactions. The beam size was on the order of 0.2 mm. 2D SAXS also probed the anisotropy in CNC suspensions by observing the intensity of the scattering pattern.

Monosaccharide analysis of pulps and papers

The carbohydrate composition of cellulosic materials governs the development of its hierarchical fibrillar structures and how they interact with external influences. Therefore, monosaccharide analysis was performed using high performance anion exchange chromatography (HPAEC) to provide a detailed breakdown of BSKP and BHKP wood pulps utilized in **Paper II** as well as key insights into xylan adsorption and degradation in **Paper IV**. All substrates were subjected to complete hydrolysis in 72 % sulfuric acid according to Theander and Westerlund (1986) before monosaccharide analysis.[106] NaOH and NaOH/NaOAc were used as eluents and fucose was used as the internal standard. Finally, saccharides were corrected for hydrolysis yields and Klason and acid soluble lignins were quantified via gravimetric and UV spectroscopy methods, respectively.[107]

3.3 Wet-State Structuring

Rheological behaviour of CNC-TBA suspensions

Rheological techniques are utilized to observe how fluids deform or flow in response to an applied force. In **Paper III**, shear viscosity and strain sweep measurements were performed on mixtures of CNCs, TBA and water to understand how interactions between components affected wet-state structural integrity. Shear viscosity measured resistance to flow at shear rates of 0.015-1000 s^{-1} and 10-1000 s^{-1} for suspensions with and without CNCs, respectively. Strain sweeps measured the elastic or plastic response of the fluids by increasing the amplitude of deformation from 0.01% to 800% at a frequency of 1 Hz. The curves representing the elastic response, or storage modulus (G') and the plastic response, or loss modulus (G'') can be used to understand the flexibility and resilience of the fluid structure by observing where these curves cross. While $G' > G''$, the fluid has a gel-like structural composition, which eventually breaks with increasing strain amplitude.

Foaming behaviour of cellulose-SDS solutions

The addition of PA and CA to fiber suspensions introduced charged molecules, leading to particular foaming patters when forming frothed fiber foams in **Paper II**. Therefore, foaming studies were conducted to understand changes in foamability, maximum achievable foam height and foam stability as a result of ionic interactions. Foamability was defined as the rate at which the volume increased until a maximum foam height was reached (H_{max}). When mechanical agitation was stopped, the gradual collapse of the bubble structure dictated the foam stability.

A model system was employed using CMC, SDS and the acid additives without wood pulp fibers. Fibers were excluded as chunks of fibrous wet foam would inadvertently trap large air pockets or stick to walls, causing issues during foaming and when analyzing results. An overhead stirrer equipped with a bladed propeller mixed components together and foamed the solutions at 1500 rpm for 20 minutes until a maximum foam height was achieved. A video camera recorded the change in foam height during foaming and collapse.

3.4 Solid Foam Properties

Density and porosity

While all solid foams produced in **Papers II, III and IV** were calculated and created to reach certain densities, unequal material distribution and shrinkage effects within the wet foam inevitably led to inter- and intra-batch variations in density. Differences in density cause changes in foam properties requiring normalization to what Gibson and Ashby (1988) refer to as relative density.[9] Relative density can be calculated via Equation 3.2:

$$\rho_{\mathrm{R}} = \frac{\rho_{\mathrm{E}}}{\rho_{\mathrm{S}}} \tag{3.2}$$

where (ρ_{R}) is relative density, (ρ_{E}) is envelope density and (ρ_{S}) is skeletal density. Skeletal density (ρ_{S}) was measured in a gas displacement pycnometer.

As relative density represents the material fraction within the solid foam, porosity, or the gas fraction, could be calculated using Equation 3.3:

$$\mathrm{Porosity}(\%) = (1 - \rho_{\mathrm{R}}) \cdot 100 \tag{3.3}$$

Structure visualization

Scanning electron microscopy (SEM) enables visualization on a micron to nanometer scale. SEM operates by beaming electrons onto a substrate surface and detecting scattered electrons. Secondary electrons are generated as a result of inelastic scattering of the beam electrons with atoms, giving topological information. Electrons that are elastically scattered are known as back-scattered electrons, and principally show changes in the chemical composition. Solid foams were cut open using a thin blade to maintain the internal structure. The foams were set to rest in a dessicator for at least 24 hours before sputter-coating a 4 nm thick layer of gold. At an acceleration voltage of 5 kV, distinct features could be visualized without destroying the structural integrity.

Mechanical testing

The change in mechanical properties in **Papers II and III** were evaluated via quasi-static mechanical compression. In this method, a load cell compresses the foam at a rate of 5 mm/min and reads the normal force applied back to the transducer. The force applied over the surface area of the foam is referred to as stress and is measured in Pascals (Pa). The deformation of the foam, or strain, is given as the displacement over the total height (%). Plotting the stress-strain curve as shown in Figure 4.11 provides insights into the behaviour of the foams under compression. At low strains, the foam structure will behave elastically as stress rises proportional to the strain. Compressive or elastic modulus provides information on foam stiffness during the initial 10% strain by taking the slope of the tangent line to the curve. The structure will eventually yield or buckle, creating a plateau where the foam deforms plastically with little resistance. The strength of the foam is taken as the stress at 10% strain, since this plateau is reached consistently before 10% strain for the cellulose fiber foams produced in this thesis. As the strain reaches 50%, densification occurs, where pores within the foam are completely collapsed and stress rises dramatically. The total energy absorbed by the foam up to this point is taken as the area under the stress-strain curve. Testing was conducted until densification was reached at 1 kN or 70 % strain. Before testing, foams were conditioned at 23 °C and 50 % relative humidity for 24 hrs according to ISO 187 before testing and a pre-load force was applied to account for any irregularities in the top layer.

Handsheets produced in **Paper IV** were evaluated though tensile properties. In this method, substrates are pulled apart in comparison to compression. Differences in short-span compression (SCT), Scott Bond internal bond strength, and Zero-span tensile strength were analyzed to determine how enzymatic degradation or adsorption of xylan affected cellulose fiber network properties.

Surface area

Nitrogen (N_2) gas physisorption is a technique providing information on specific surface area and pore sizes less than 200-300 nm in CNC foams produced in **Paper III**. (N_2) gas is released into a cell with the substrate where it adsorbs onto available surfaces. At relative pressures up to 0.3 $p/(p_0)$, a monolayer of nitrogen atoms is formed on all surfaces and micropores (< 2 nm) are filled. In the range of 0.05 - 0.3 $p/(p_0)$, the surface area can be quantified using the Brunauer-Emmett-Teller (BET) equation:[108]

$$\frac{\frac{p}{p_0}}{n(1-\frac{p}{p_0})} = \frac{C-1}{n_\mathrm{m}C}(\frac{p}{p_0}) + \frac{1}{n_\mathrm{m}C} \tag{3.4}$$

where for the adsorbate (N_2), p is the equilibrium pressure, p_0 is the saturation pressure, n is the amount of N_2 adsorbed, n_m is the monolayer capacity, and C is the BET constant. By plotting Equation 3.5,

$$\frac{1}{n(\frac{p_0}{p})-1} \tag{3.5}$$

over the relative pressure ($p/(p_0)$), the slope (s) and y-intercept (i) can be used to find n_m and C:

$$n_\mathrm{m} = \frac{1}{s+i} \tag{3.6}$$

$$C = \frac{s}{i} + 1 \tag{3.7}$$

ultimately allowing calculation of specific surface area:

$$SSA = \frac{n_\mathrm{m} * N_\mathrm{A} * \sigma_\mathrm{m}}{V_0 * m} \tag{3.8}$$

where N_A is Avogadro's number, σ_m is the molecular cross sectional area (0.162 nm^2 for N_2), V_0 is the molar gas volume and m is mass. The continued adsorption of nitrogen as multilayers fills larger pores until the saturation pressure is reached. A desorption curve is measured as the sample is heated to release nitrogen from the surfaces. From the hysteresis present during desorption, information regarding pore shape and size can be determined.

Thermal degradation

In **Papers I and II**, reaction of phytic acid cross-linked fibers to heat and fire showcased the value of phosphorylation toward fire resistance. Thermo-oxidative degradation behaviour was analyzed via thermogravimetric analysis (TGA), which measures the mass loss of substrates when exposed to temperature changes. Under air flow, the material was exposed to a temperature ramp from 30 °C – 800 °C at a rate of 10 K/min followed by a hold for 10 mins. Characteristic changes in the graph include: Carbonization onset, weight loss and rate of carbonization, degradation rate, and residual weight.

Fire retardancy

Cone calorimetry was used to quantify the flammability and fire-retardancy of foams reacted with phytic acid in **Paper II** according to ISO 5660-3. By applying a medium thermal attack (controlled fire) to the substrate, combustion of the material leads to heat release and soot generation. Analyzing these enables an accurate determination of time to ignition (TTI: sec), peak heat release rate (PHRR: kW/m^2), fire growth rate (FGR: $kJ/m^2/s$), total heat release (THR: MJ/m^2), total smoke production (TSP: m^2) and smoke production rate (m^2/s). Together, these values are used for regulation demanded fire classification of materials.

CHAPTER 4

Results and Discussion

The key components which underline this work are cellulose and the formation of a porous network. Therefore, an understanding of how each of these components influences the structural stability is necessary. Here, the fundamental concepts behind how fiber and pore morphology are formed and lend mechanical strength to cellulose fiber foams are elucidated and solutions are presented.

4.1 Cellulose - Phytic Acid Interactions

4.1.1 Modification of Cellulose

Phytic acid (PA) was heat treated on cellulose fibers to catalyze dehydration synthesis; a form of condensation reaction in which water is removed. The goal was to covalently cross-link PA and cellulose through the formation of an ester bond. To overcome entropic effects associated with the formation of this linkage in aqueous media, heat was applied to drive a nucleophilic attack by hydroxyl (OH) groups. The expected outcome was that of product 3 in Figure 4.1, where cellulose OH groups attack the highly electronegative phosphorus atom in PA phosphate groups.[109,110] However, we considered two alternate products resulting from inter- and intra-phosphate reactions.

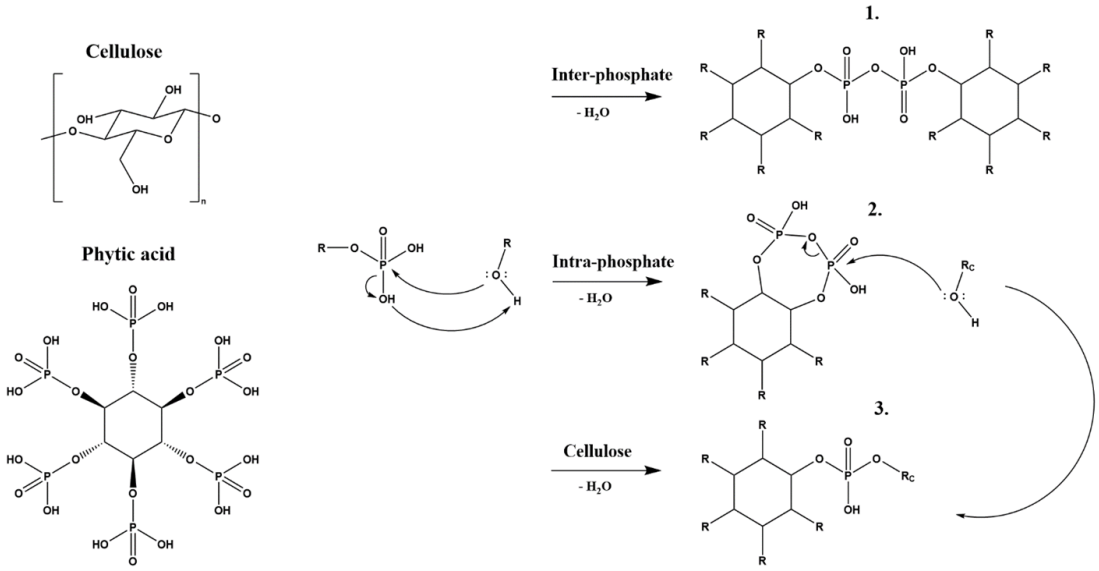

Figure 4.1: Proposed mechanisms for phytic acid-cellulose condensation reactions. R = phosphate groups (PO_3-H) or C2, C3 or C6 of cellulose. RC is defined as specifically C2, C3 or C6 of cellulose. Reproduced from Orzan et al. under Creative Commons CC-BY license.[111]

Phosphate OH groups are more nucleophilic than cellulose OH, and are therefore susceptible to attack from other phosphate groups. In a system with sufficient nearby PA molecules, product 1 is the predominant outcome due to inter-phosphorylation, and leads to the formation of polymeric oligo-phosphate chains.[79,110] To overcome this, our study employed a significantly lower con-

centration of PA (0.04 M) compared to the literature.[74,112–115] Even at low PA concentrations, we hypothesized that intra-phosphorylation reactions occur as a result of the spatial arrangement of phosphates in the molecule. The outcome is the formation of a cyclic anhydride similar to citric acid (CA) shown as intermediary product 2.[72,73,82,98,116] However, cyclic anhydrides are highly reactive, making them susceptible to nucleophilic attack by cellulose OH groups.

Successful cross-linking of phytic acid would transform phosphate mono-esters into di-esters, generating peaks at -2.0 and -3.0 ppm in solid-state ^{31}P NMR spectra (Figure 4.2a).[109,112,117] Deconvolution of the spectra revealed three overlapping peaks at 0.5, -0.7, and -2.0 ppm with a series of minor peaks further upfield. Integrating over the peak areas at -2.0 and -3.0 ppm revealed a relative increase in area of 13% for P20U (dried at 20 °C and unwashed) to 24% for P160W (dried at 160 °C and washed). As such, the heat-treated P160W substrate presented a pronounced shoulder at -1.3 ppm compared to the unreacted P20U spectra. Moreover, the characteristic peak for PA phosphate mono-esters at 0.5 ppm decreased in relative area from 48% to 28%, confirming the formation of di-ester covalent cross-linking. Tri-ester and oligo-phosphate peaks, which typically present further upfield from -3.0 ppm, accounted for 9% of the spectra in P160W. On the other end, downfield peaks from 1.5 to 7.5 ppm showed negligible changes, indicating a lack of discernible dephosphorylation or degradation to ortho- and pyro-phosphates.[118]

Solid-state ^{13}C NMR was unable to support any conclusion as phosphates bound to cellulose chains produced overlapping peaks and comprised only a small fraction of PA-based carbons in the substrate (Figure 4.2b). Investigation of FTIR spectra in Figure 4.2c revealed a decrease of 3% in the shoulder intensity at 900 cm^{-1} ($\delta_{\text{P-OH}}$) when normalized to the band at 1245 cm^{-1} ($\delta_{\text{P=OH}}$).[110,117] This suggests that for each phosphate, the amount of P-OH bonds has decreased to form the ester bonds found in ^{31}P NMR. Direct probing of C-O-P bonding in FTIR is challenging due to the overlap with C-O-C stretching from 980 - 1160 cm^{-1} ($\delta_{\text{C-O}}$). Yet, taking 1030 cm^{-1} as a representative band for C-O-P and normalizing it by P=O indicated a nominal increase of 2% for P160W over P20U. Overall, the combination of ^{31}P NMR deconvolution and FTIR analysis strongly suggested the formation of phosphate di-esters. Subsequent elemental analysis of the heat-treated cellulose substrates confirmed the cross-linking action of PA to cellulose.

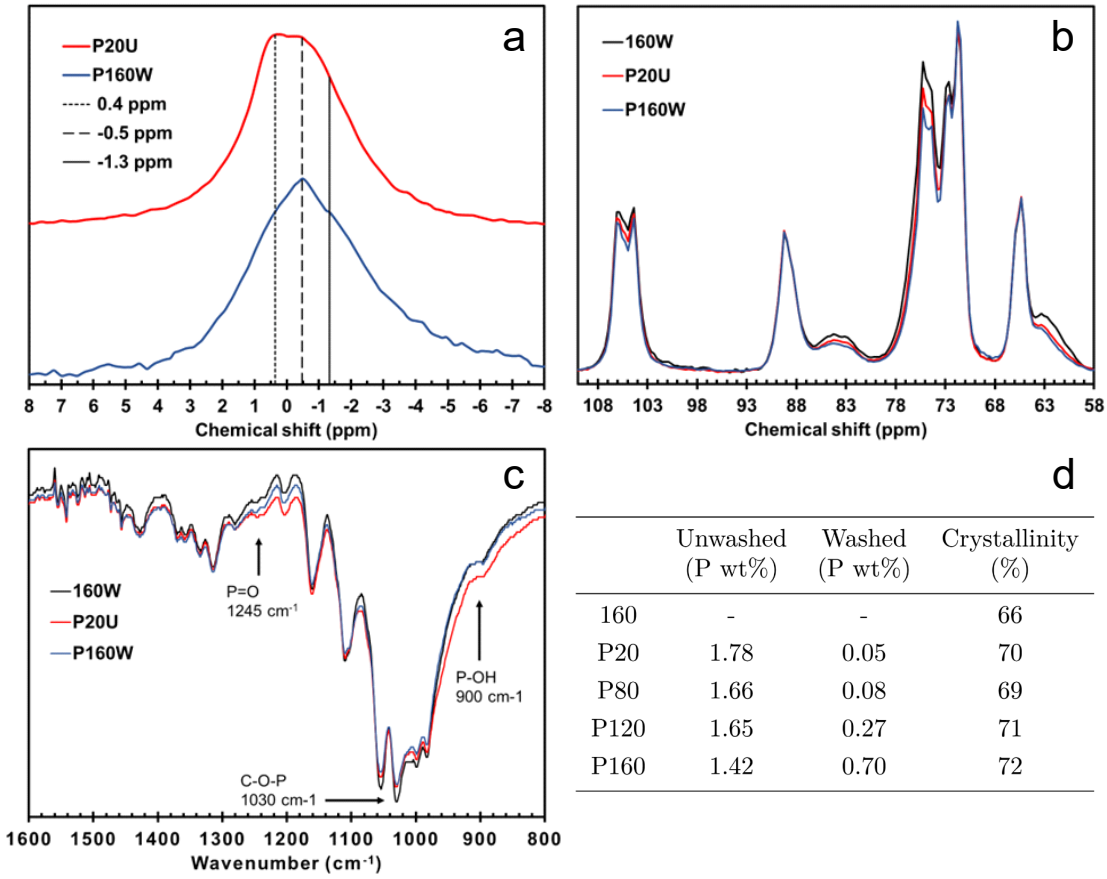

	Unwashed (P wt%)	Washed (P wt%)	Crystallinity (%)
160	-	-	66
P20	1.78	0.05	70
P80	1.66	0.08	69
P120	1.65	0.27	71
P160	1.42	0.70	72

Figure 4.2: Comparison between the cellulose substrates treated at 160 °C and washed (160W), reacted with PA (P160W), and dried at RT with PA without washing (P20U) using a) ^{31}P NMR, b) ^{13}C NMR, c) FTIR, and d) phosphorus content and cellulose C4 crystallinity. Reproduced from Orzan et al. under Creative Commons CC-BY license.[111]

Washing of the cellulose substrates removed unreacted and dephosphorylated molecules, leaving only cross-linked phosphates. The washed column in Figure 4.2d demonstrated this as an increased retention of phosphates at higher reaction temperatures. P20W and P80W retained trace phosphorus content, indicating a lack of strong covalent bonding and the inability of hydrogen bonding to retain PA molecules on cellulose. Notable dephosphorylation to gaseous phosphoric acids was observed through decreasing phosphorus content on unwashed substrates. Heat treatment at 160 °C triggered a dip as the onset of PA thermal degradation was reached.[119]

Change in cellulose crystallinity

The application of PA to fibers led to critical changes in cellulose fiber crystallinity, which became relevant when discussing their transformation into fiber foams. In ^{13}C NMR, the C4 carbon of cellulose presented two distinct peaks: crystalline (89 ppm) and non-crystalline (84 ppm) structures (Figure 4.2b).[104,120,121] Simply applying PA to the cellulose substrate in P20U led to an increase in crystallinity of 4%. This can be ascribed to the degradation of non-crystalline regions through acid hydrolysis by phosphate-based acids.[70,71,122] Upon heat treatment, PA dephosphorylation likely caused the further increase in crystallinity.

Wickholm and Larsson (1998) deconvoluted NMR signals in the C4 region to explain cellulose structures.[121] The broad signal presenting at 84 ppm contained two minor peaks within; depicted as accessible fibril surfaces surrounding crystalline regions (Figure 4.2b). The action of PA decreased their intensity, which can be explained by the following mechanisms:

i) Covalent bonding of phytic acid to cellulose forming para-crystalline structures between cellulose fibrils and reducing accessible surfaces.

ii) Hydrolysis of non-crystalline regions surrounding the crystalline core.

Therefore, the decreased crystallinity in cellulose fibers is credited the degradation of accessible non-crystalline structures in the outer sheath and inaccessible ones between crystalline regions. Visualization using SEM suggested a reduction in cellulose micro-fibrils and the formation of cracks in larger fibers, consistent with reports in literature.[112,123,124]

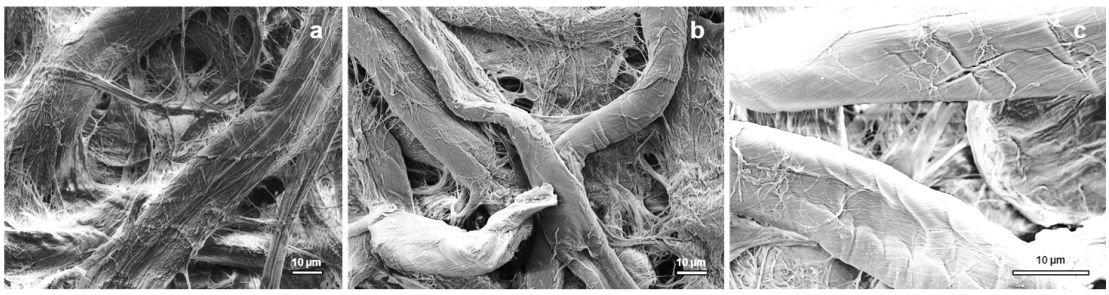

Figure 4.3: SEM of cellulose substrates a) 160W, b) P20U, and c) P160W. Reproduced from Orzan et al. under Creative Commons CC-BY license.[111]

4.1.2 CMC-SDS Foaming

The cellulose fiber foams produced in Paper II were foamed and stabilized using a combination of CMC and SDS. The resulting structure and foaming behaviour warranted investigation via wet foam analysis (Figure 4.4i, ii). Adding PA to solutions of CMC + SDS increased foamability by 35% and produced larger volumes of foam, $H_{\max}$ (Table 4.1 and Figure 4.4). However, when mixing was stopped, the volumetric rate of foam collapse doubled. Therefore, PA changed the behaviour of the system by reducing pH and interacting with CMC.

Table 4.1: Wet foam analysis where $H_{\max}$ represents the maximum foam height and t_{20} describes the time to reach 20% of $H_{\max}$ after foaming. Reproduced from Orzan et al. under Creative Commons CC-BY license.[125]

Foam additives[1]	$H_{\max}$ (mL)	Foamability[2] (mL/min)	t_{20} (min)	Stability (mL/min)	pH
SDS	308	310	523	-0.47	6.4
SDS + PA	298	290	150	-1.55	1.6
CMC + SDS	152	350	419	-0.29	7.1
CMC + SDS + PA	184	470	216	-0.68	2.0
CMC + SDS + CA	187	500	443	-0.34	3.2

[1] Phytic acid by itself showed no foaming behaviour and thus is not included.
[2] Foamability describes the volume of foam within the first 30 seconds as a rate.

Compared to just CMC, solutions of CMC + PA have shown increased viscosity due to hydrogen bonding and formed gel-like structures.[126] This enhanced gas bubble encapsulation during mixing, allowing for a greater volume of foam to be generated. The viscosity also reduced both the rate of drainage from lamellae between the bubbles and the diffusion of gas causing coarsening. The resulting stability of the wet foam and bubble formation produced a visible opacity in the CMC + PA solution (Figure 4.4iii and iv). Moreover, the increased stability of CMC + SDS compared to SDS solutions gives credence to this conclusion. Adding PA to SDS solutions led to negligible changes aside from a slight delay in $t_{\max}$. Therefore, during mixing, changes in foamability and foam height are credited to the combination of CMC and PA introducing viscous effects which: i) improved foam stability by reducing drainage and coarsening and ii) increased foamability via gas bubble encapsulation.

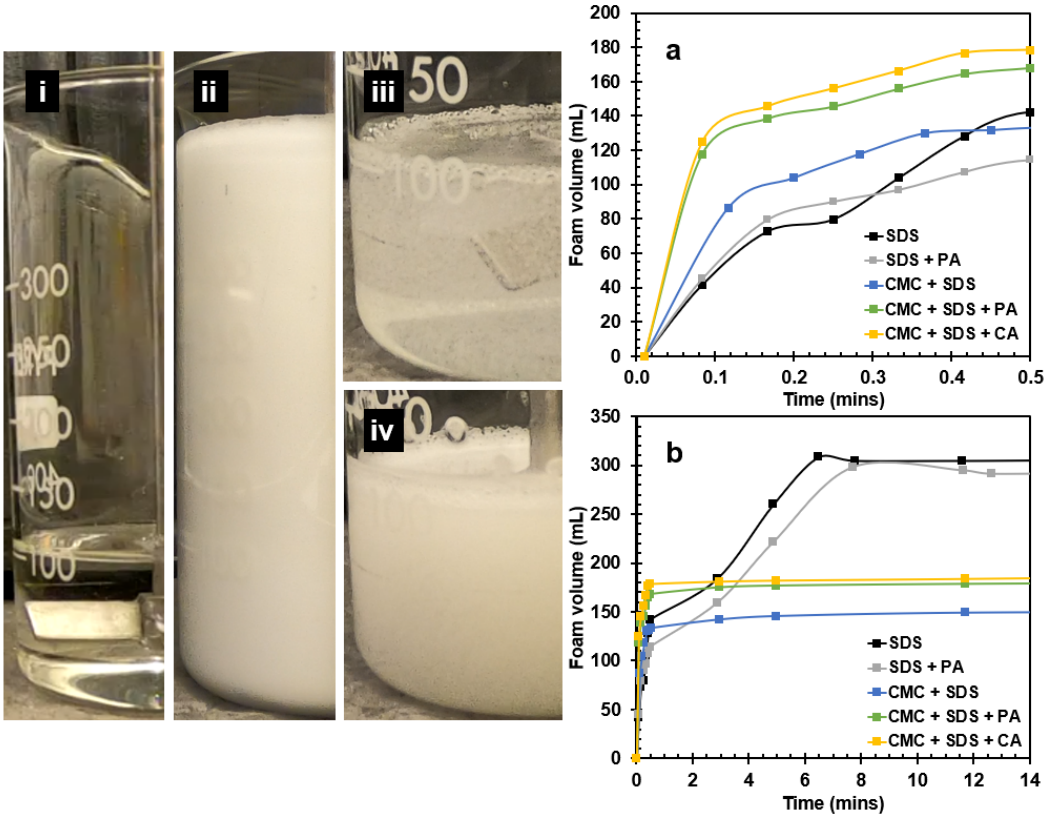

Figure 4.4: Wet foam analysis during mixing where i = setup, ii = SDS + PA at 18 min, iii = CMC at 18 min, iv = CMC + PA at 18 min. a and b) foam volume at short and long time-scales. Reproduced from Orzan et al. under Creative Commons CC-BY license.[125]

As mixing stopped and lamellae drained, a 2-3 fold increase in the foam collapse rate was observed for solutions containing PA (Figure 4.5a). PA dropped the pH of the solution below 2, leading to the protonation of both SDS and CMC (CMC pKa $\approx$ 4.5, SDS pKa $\approx$ 3.3).[127,128] With fewer repulsive electrostatic interactions within the drained lamellae, disjoining pressure between bubbles was reduced. Therefore, the energy barrier toward film rupture was more easily overcome and bubble coalescence slowly destabilized the foam structure, causing rapid collapse (Figure 4.5i-iv). Viscous effects of CMC produced a stable plateau until 100 minutes after foaming and reduced the overall rate of collapse compared to solutions with only SDS. Furthermore, the addition of acids increased the rate of drainage (Figure 4.5b). This can be explained from gravitational effects on the denser solutions, yet other effects relating to diffusion may influence this phenomenon as well.

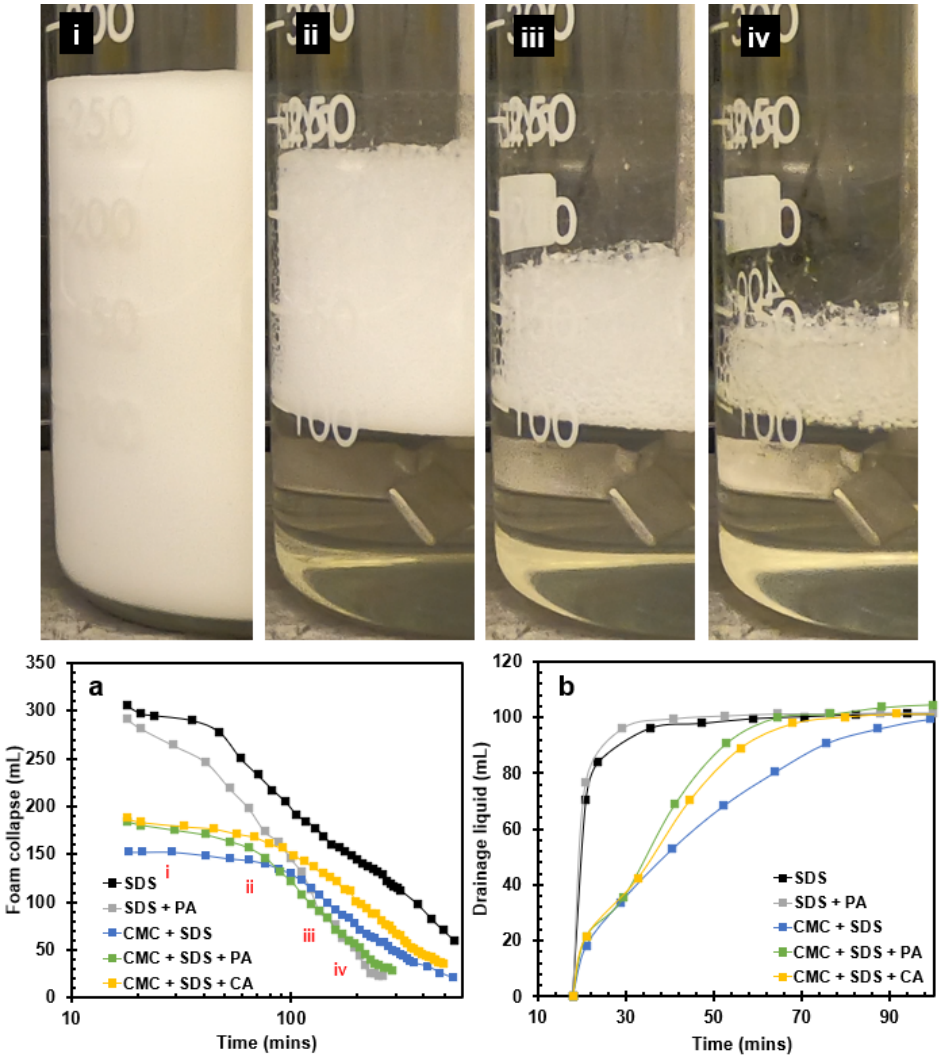

Figure 4.5: Foam collapse starting at 18 min (i - iv = CMC + SDS + PA at 18 min, 1 hr, 2 hrs, 3 hrs, respectively. Reproduced from Orzan et al. under Creative Commons CC-BY license.[125]

CA produced nearly identical results to PA foaming. The principle difference lies in the foam stability, which was mostly unaffected compared to CMC + SDS foams, unlike with PA. As a weak acid, CA reduced the solution pH to 3.2, possibly leaving some SDS molecules deprotonated and negatively charged. A similar w/w addition to PA also led to 3-4 times more CA molecules. Therefore, the combination of increased electrostatic repulsion and hydrogen bonding in CA systems created foams with both high foamability and stability.

4.2 TBA-Induced Structuring of CNCs

4.2.1 Suspension Assembly and Rheology

Despite begin considered miscible in water, TBA forms nano-scale disturbances in the liquid-phase structuring of water.[46,49,129–132] TBA hydroxyl groups hydrogen bond with water while their large tertiary aliphatic groups are driven towards hydrophobic interactions. Therefore, dynamic regions of TBA and water are formed: micellar-like regions with large concentration differences, and bicontinuous microemulsions around 30-50 wt% TBA.[46,49,129] When adding CNCs to solutions of TBA and water, it is not clear how or if structuring will be affected. Analysis of WAXS patterns was inconclusive to this end. The diffraction peaks of cellulose I_β (200, $1\bar{1}0$ and 110) at $q = 1.6$ Å^{-1}, and between $q = 1.0$ and 1.2 Å^{-1} were probed to see changes in CNC-CNC distances (Figure 4.6a). However, addition of 30 and 46 wt% TBA masked peak changes as scattering of aliphatic interactions of TBA also occurs around 1.25 Å^{-1}. TBA-water structuring was relatively unchanged at 2 and 0.5 Å^{-1}. The upturn below 0.5 Å^{-1} when CNCs are present corresponds to the start of mesostructure scattering in the SAXS range.

A distinct change in SAXS scattering was perceived when adding >30 wt% TBA to CNC suspensions. The peak corresponding to inter-CNC packing distances at 0.01-0.02 Å^{-1} and the shoulder at 0.02-0.05 Å^{-1} in the 1D SAXS intensity pattern became less pronounced (Figure 4.6b,c).[133,134] Beginning at 40 wt% TBA, the lamellar periodic structuring originating from CNC ordering in water was altered. Where once a parallelepiped form factor with a hard-sphere structure fit the curve of CNC-water suspensions, 50 wt% TBA had to be modeled as polydisperse parallelepipeds without a hard-sphere factor.[135] Because of this, the effective radius of CNC packing could no longer be determined as CNC assembly became less ordered and a percolated network was formed. A shift from anisotropic to isotropic alignment at >30 wt% TBA could be determined from circularly averaged 2D SAXS intensity patterns at CNC concentrations >3 wt%. A schematic representation of this structural change is presented in Figure 4.7a,b,c.

The disturbance in the ordered packing of CNCs produced distinctly featureless curves. At low q, a steeper slope of q decay was also observed, indicating the presence of aggregated clusters of smaller structural subunits (Figure

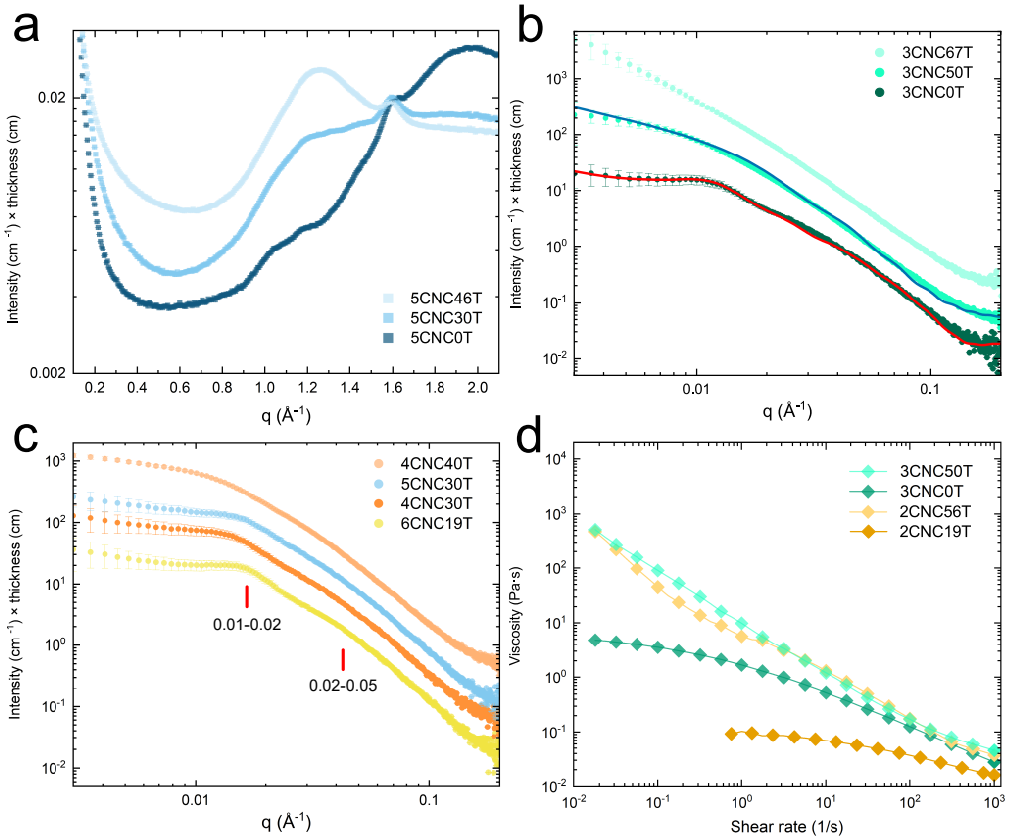

Figure 4.6: Analysis of suspensions using a) WAXS, and b,c) SAXS. The lines in b signify fits to a parallelepiped form factor with (red) and without (blue) hard-sphere structure. The red line in c) shows representative peaks for CNC packing distance. d) Shear viscosity measurements.

4.7d). The previously constant q decay between $q^{-0.2}$ and $q^{-0.6}$ transitioned to q^{-1} at 50 wt% TBA and progressed to $q^{-2.2}$ at 67 wt% (Figure 4.7a). In all, regardless of CNC concentration, increasing TBA concentration caused the CNC network to forgo ordered packing in favor of percolated structures and subsequently to larger aggregated clusters.

The rheological behaviour of TBA-water systems was likewise unaffected by <40 wt% addition of TBA. The Newtonian plateau at low shear rates suggested isotropic shear behaviour with the addition of up to 4 wt% CNC. As the ordered packing of CNCs became disturbed in SAXS, the suspensions exhibited a rising viscosity and storage modulus (G') and a decreasing damping factor tan δ (Figure 4.7e). These results signified a transition to a more elastic

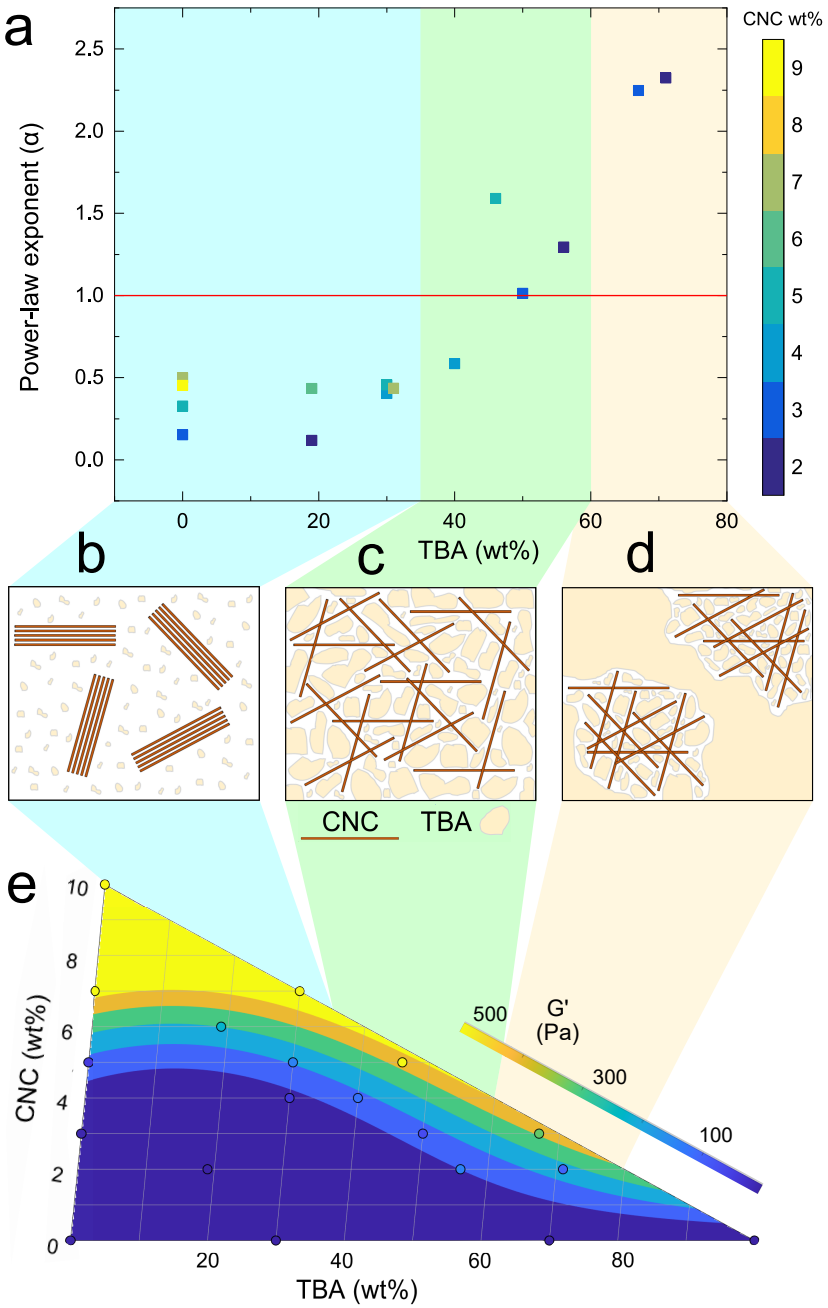

Figure 4.7: Combination chart of a) the power-law exponent, α, as a function of TBA content. The red line denotes the transition from ordered CNC packing ($\alpha \leq 1$) to increasing degrees of aggregation. b-d) Schematic representation of CNC assembly. e) Ternary contour plot of G' (Pa) in the linear region during strain sweep measurements.

network above 30 wt% content of TBA. The interaction between percolated CNCs led to a cross-over point between storage (G') and loss modulus (G''), signifying greater structural stability of the suspensions. Above 60 wt% addition of TBA, suspensions broke and phase separation occurred gradually.[136] The volumetric presence of TBA at this concentration enveloped CNC-water regions, forming disparate clusters due to depletion flocculation.[137] The mechanisms by which the structuring and stability of CNC-TBA-Water suspensions developed are therefore proposed as follows:

i) TBA forms nanoscale liquid structures with water, decreasing the relative permittivity of the medium.[138,139] The lower polarizability leads to increased screening of the electric potential between charged CNCs, reducing the Debye length. The reduced Debye length causes CNCs to converge, increasing the likelihood of inter-CNC hydrogen bonding thus forming stronger interparticle interactions in the network.

ii) Tertiary aliphatic groups of TBA adsorb onto hydrophobic CNC interfaces, resulting in augmented CNC hydrophilicity as TBA hydroxyl groups permit hydrogen bonding to the bulk water phase.[140,141] The adsorption is a spontaneous thermodynamic process as both entropy and enthalpy drive the removal of water molecules from surfaces in favor of hydrophobic CNC-TBA interactions.[142–144] Therefore, attractive London and van der Waals forces and long-range electrostatic repulsions are suppressed, dispersing CNCs into isotropic percolated networks.[145]

4.2.2 Cryogel Surface Area and Porosity

Nitrogen adsorption for all CNC cryogels developed type II isotherms. A steep increase at low relative pressure indicated filling of micropores (<2 nm diameter) before transitioning into the linear BET area (Figure 4.8). From approximately 0.05 - 0.35 relative pressure, specific surface area (SSA) could be estimated using the BET theorem (Equation 3.8) as adsorbate covered surfaces of meso- (2-50 nm) and macropores (>50 nm). The exponential rise in volume past this region suggests a wide distribution of mesopore sizes. The asymptotic increase starting at around 0.8 relative pressure and a lack of a Gurvich plateau indicated incomplete filling of macropores. The desorption branch exhibited type H3 hysteresis without loop closure, confirming plate-like or tubular porous structures causing capillary evaporation.[146]

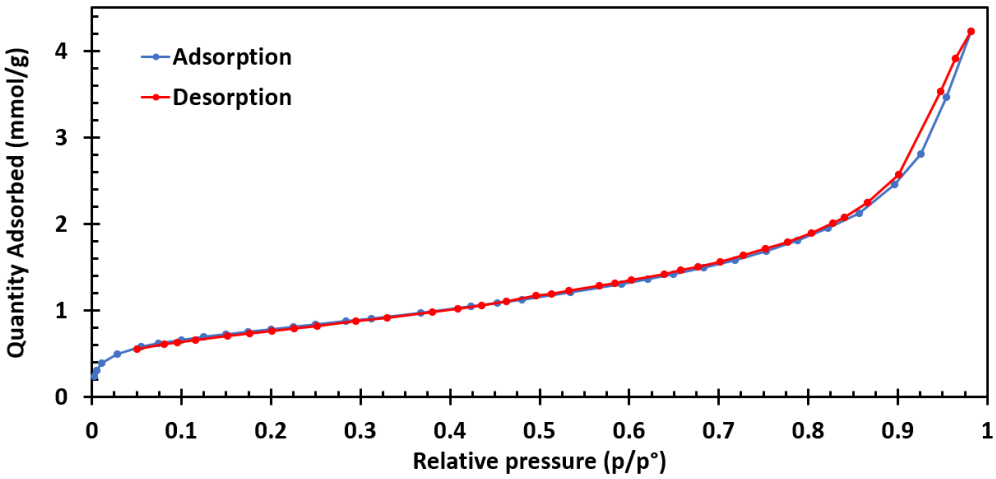

Figure 4.8: Nitrogen adsorption and desorption curves for 3CNC50T.

A direct relationship between porosity or SSA and CNC concentration in the cryogels was clear. Increasing CNCs filled the pore spaces and were forced to pack closer within the pore walls. Cryogels formed without the influence of TBA presented the lowest SSA; particularly above 5 wt% as CNCs spontaneously self-assembled into nematic structures due to entropic forces. The flat, sheet-like morphology confirms the reason for low SSA (Figure 4.9a). The SSA of 3 wt% CNCs was 15 m^2/g, while 5-10 wt% exhibited less than 5 m^2/g. These values are in line with results described for other CNC cryogels presented in literature.[147–149]. For comparison, CNC aerogels (dried with supercritical CO_2) and CNF cryogels showed SSA over 150 m^2/g due to the drying process and fibrillar nature, respectively.[149–151]

Freezing of suspensions containing TBA led to a universal increase in SSA as TBA-water interactions induced smaller crystal formation. This was particularly apparent at 20 and 70 wt% TBA where cryogels obtained SSA above 70 m^2/g and the developed visible mesoporosity (Figures 4.9b,d). Fumagalli et al. (2013) found a direct correlation with increasing TBA concentration up to 80 wt% and CNC cryogel SSA.[147] However, they did not report a significant rise in SSA at 20 wt% TBA, contradicting our results. This may be attributed to the discrepancy in CNC concentration (1 wt% in Fumagalli et al.) In CNF cryogels, a similar correlation was found.[152,153]

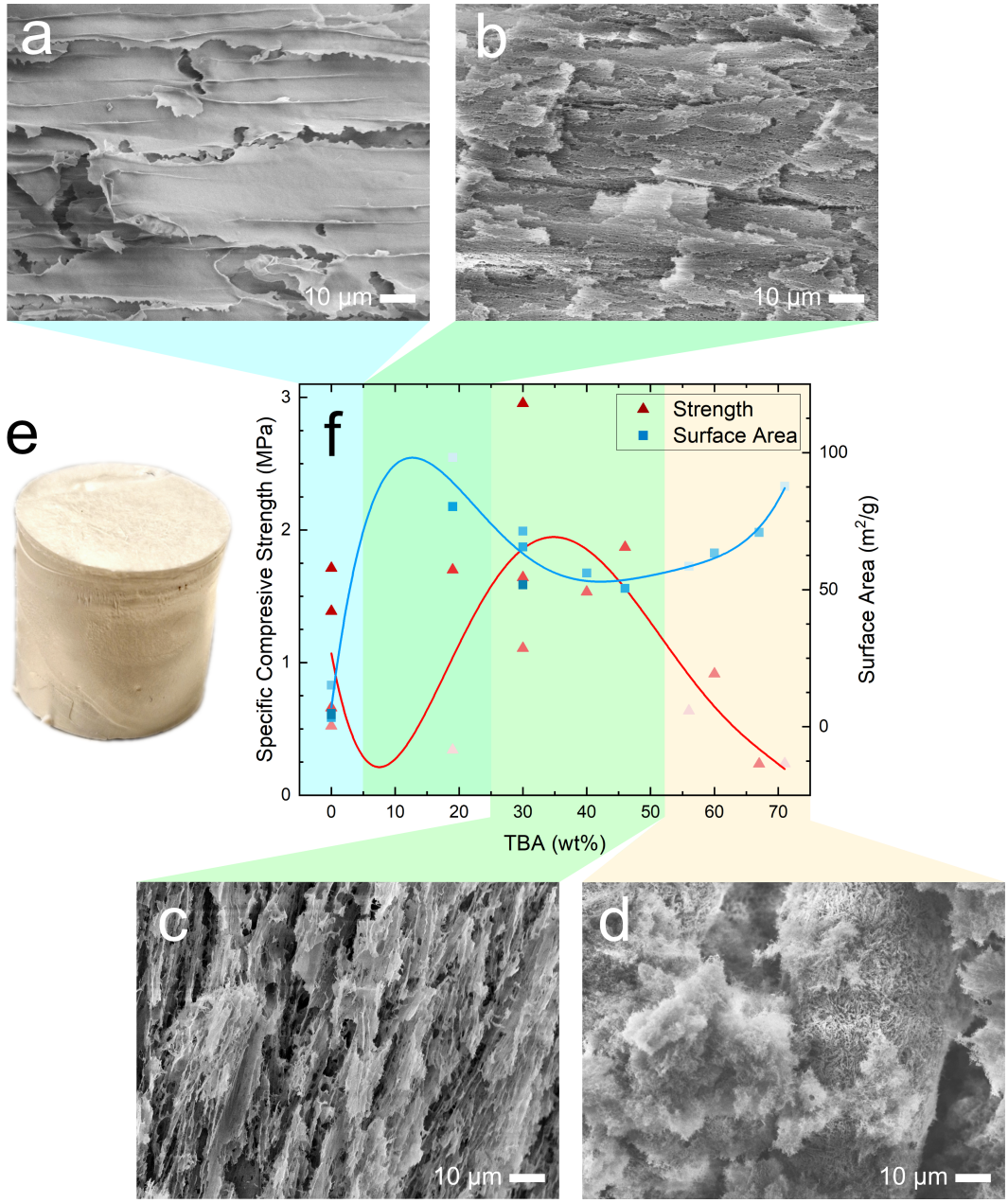

Figure 4.9: Morphologies of CNC solid foams observed via SEM for a) 0 wt% TBA (sheet/lamellar), b) < 30 wt% TBA (porous lamellar), c) 30-50 wt% TBA (tubular), and d) > 60 wt% TBA (aggregated). The correlation between SSA and specific compressive strength with respect to TBA wt% is presented in f).

4.3 Strengthening of Cellulose Networks

In the interest of strengthening cellulose foams, approaches toward i) pore structure formation, and ii) covalent or physical cross-linking were evaluated. Using TBA to control crystal formation during freezing, a spectrum of structural morphologies could be attained. This method gives insights into the role of pore structures on compressive behaviour. On the other hand, fiber networks were analyzed by looking at the degradation of cellulose fibers from enzymatic or PA treatment. Using the covalent di-ester bonds formed between PA and cellulose or adsorbing extrinsic xylan, an evaluation of how these phenomena affect foam mechanical properties was obtained.

4.3.1 Morphological Transformations of CNC-TBA Cryogels

The structuring of freeze-dried cellulose cryogels using TBA is well documented with regards to the effect on SSA.[147,149,152] However in Paper III, we exploited the unique ice crystal formation to document how the changing morphology affected the compressive behaviour of CNC cryogels. Without TBA, ice crystals pushed CNCs into the interstitial areas and formed densified lamellar sheets (Figure 4.9a). As CNC concentration increased from 3 to 10 wt%, a clear rise in compressive modulus, strength, and energy absorption was observed as CNC aggregation within pore walls increased inter-crystal connectivity (Table 4.2). This strengthening effect was also documented by Tripathi et al.[154] and Ruiz-Caldas et al.[148] for CNC foams dried by supercritical CO_2 (4-7 wt% CNCs) and freeze-drying (3-5 wt% CNCs), respectively. The specific compressive moduli of 10-20 MPa obtained in our study were markedly similar to the values obtained by Ruiz-Caldas et al. at concurrent CNC concentrations. A 10-fold improvement over supercritically dried foams from Tripathi et al. showcases how increased SSA leads to a reduced structural strength. Darpentigny et al.[149] produced cryogels with 1 wt% tunicated CNCs which were solvent exchanged with an 80/20 mixture of TBA/water. These foams showcased an impressive 18 MPa modulus for their weight, credit to their "netted" morphology".

In the range of 30-50 wt% TBA, the cryogels produced in our study had a notably similar "netted" morphology, described as tubular, capillary or needle-like (Figure 4.9c). Compared to sheet-like structures formed without TBA,

Table 4.2: Properties of cryogels in mechanical compression.

	Surface Area (m^2/g)	Modulus (MPa)	Energy Abs. (MJ/m^3)	Strength (MPa)
4CNC30T	71	9.0	0.83	1.1
4CNC40T	56	36	2.45	1.5
6CNC19T	80	21	1.67	1.7
7CNC0T	4.9	22	1.58	1.4
7CNC30T	52	64	4.32	3.0
10CNC0T	4.0	40	3.15	1.7

the morphology in this range depicts interconnected pore walls, providing long-range macro-structural support throughout the foam matrix. As such, a consistent 3-fold increase across all CNC concentrations was observed. The incorporation of 40 wt% TBA to 4 wt% CNCs produced cryogels with a strength comparable to 10 wt% CNCs without TBA. This demonstrated the potential for pore structuring to mechanically compensate for reduced foam mass (Table 4.2). Therefore, cryogels in this range can be tailored towards applications requiring high specific mechanical performance while maintaining a greater SSA than foams devoid of TBA.

Cryogels tailored for maximum SSA at 20 and 70 wt% TBA had little effect on mechanical properties compared to those made without TBA. The microporous inclusions disrupting lamellar sheets in Figure 4.9b and the disparate aggregates in Figure 4.9d were of no significant consequence compared to the macro-scale pore structuring. Thus, it can be surmised that the loss of fiber-fiber contacts (leading to high SSA) was compensated by an increased fibrillar network structure. Overall, an indirect relationship was apparent between mechanical properties and SSA for systems containing TBA (Figure 4.9f). These results provide a new dimension to the value of TBA in nanocellulosic cryogels and aerogels by exploring the compressive behaviour above 1 wt% CNCs.

4.3.2 Fiber Degradation / Cross-linking with Phytic Acid and Xylan

To verify how phytic acid had affected the fiber network mechanically, compression testing of cellulose fiber foams was performed and compared against CA cross-linked foams. The effect of PA degradation on the fiber network is clear when comparing the properties of the foams reacted with PA at 80 °C (P80) to the blank foam without acids (80). Stiffness, strength, and toughness all decreased simultaneously due to the addition of PA (Figure 4.10). Therefore, degradation plays a decisive role in compressive behaviour of fiber foams as the removed non-crystalline regions no longer play a supporting structural role in the fiber network.

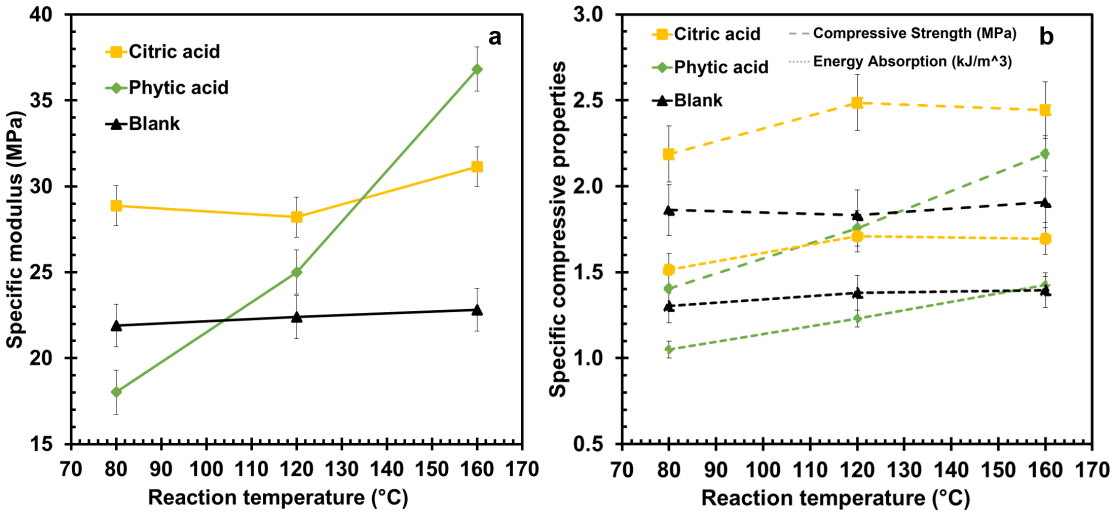

Figure 4.10: Compression testing of cross-linked fiber foams compared by a) specific modulus and b) specific strength and energy absorption. Reproduced from Orzan et al. under Creative Commons CC-BY license.[125]

Upon addition of PA, a balance is struck between cellulose fiber degradation and cross-linking due to PA and the formation of covalent bonds. The degradation (hydrolysis) removed some of the amorphous bulk surrounding each fiber, decreasing potential fiber-fiber contact area and therefore compromising the network strength. Increasing the reaction temperature to 120 °C brings the compressive properties of cellulose fiber foams with PA (P120) to equivalence with the blank foams (120) (Figure 4.10). At temperatures above 160 °C, the covalent bonds between PA and cellulose fibers drastically increased the contact strength between fibers. Comparison with cellulose fiber

foams reacted with CA at a similar temperature shows that PA can produce higher stiffness at <10% strain (Figure 4.10a). However, energy absorption of the fiber foams reacted at 160 °C with CA improved by nearly 20% over PA solid foams (Figure 4.10b).

To corroborate the effects of fiber degradation seen in Paper II, xylan was enzymatically degraded or adsorbed to cellulose fibers in Paper IV. This also allows for a comparison of reinforcement techniques via physical or chemical cross-linking. Applying an endo-xylanase to pulp fibers led to a 1% decrease in intrinsic xylan content and visible fraying of the fibers due to partial degradation. Moreover, adsorption of 3% extrinsic xylan formed minor aggregates visible on the fiber surfaces in SEM. Xylan aggregated in the aqueous solutions and then adsorbed to the outer layers of fibers in that configuration, with unsubstituted linear regions of xylan bonding to cellulose surfaces.[155–157] However, the cellulose fibers as a whole displayed no significant change in length/width, coarseness, curl, zero-span tensile strength or fibril area.

The tensile index of the fiber networks was directly correlated to xylan content. As xylan was adsorbed, handsheet density, swelling capacity and surface fiber charge were increased. These led to a strengthening effect as more fiber-fiber bonds were formed.[158–160] However, intrinsic xylan degradation was more impactful than extrinsic xylan adsorption (Figure 4.11). For each property listed, degradation of 1% xylan reduced properties more than an equivalent 1% adsorbed xylan augmented them. This effect may be explained by the aggregated form of extrinsic xylan, which has a lower potential to reinforce the fiber network. The intrinsic xylan present in fibers after pulping are therefore vital to the strength of fiber networks. This effect was not as pronounced when applied in cellulose fiber foams, as the low density nature of these networks reduced the potential for fiber-fiber bonding.[161] In addition, handsheets provided a direct and valuable observation of the fiber network behaviour without significant influence from pore structuring.

In Figure 4.11, specific mechanical properties of fiber networks developed recurring trends when fibers were reinforced or degraded. The addition of a physical or covalent cross-linking agent was most impactful on the modulus. Furthermore, the stiffness of the fiber network and its ability to deforem elastically was less affected by the loss of intrinsic structures. The opposite effect was seen in energy absorption, where degradation of native structures within cellulose fibers was more detrimental than any gains through cross-linking. This is a key revelation when considering using cross-linking in an applica-

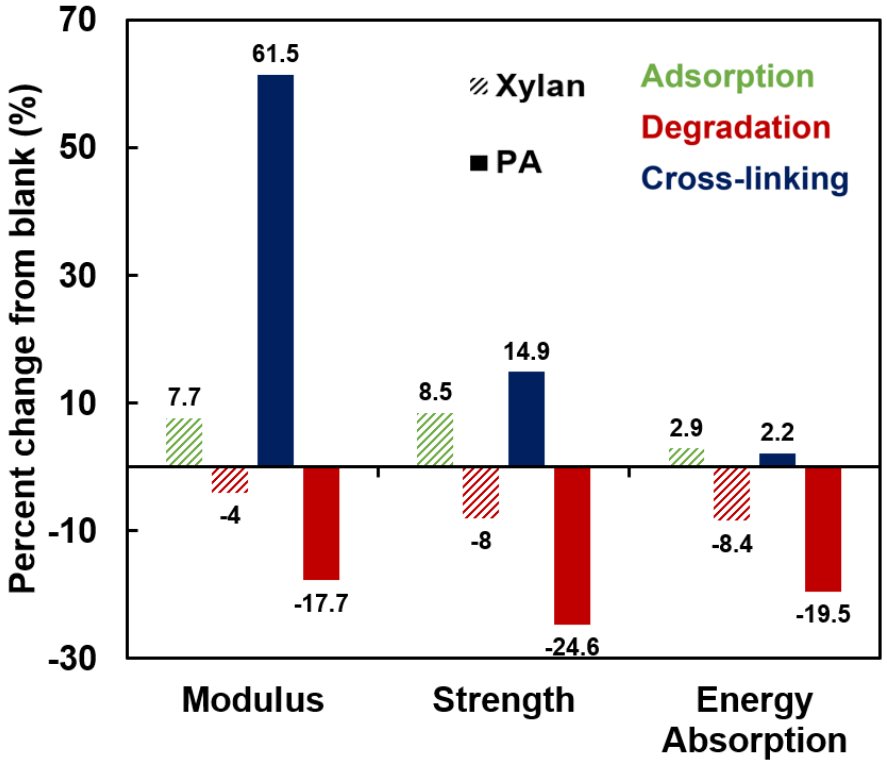

Figure 4.11: Comparison of mechanical properties for fiber networks with phytic acid degradation/cross-linking in compression and xylan degradation/adsorption in tensile.

tion requiring improvements in energy absorption. While the systems differ greatly in both material and morphology, a striking difference is seen with the structural reinforcement brought about by only 30% TBA in CNC cryogels. The relative increases in modulus (183%), strength (179%), and energy absorption (121%) are disproportionally greater than any cross-linking work performed. The rearrangement of interior structural elements seems to be the preferred method to strengthen networks of discrete fibers, especially since no extra mass is added.

4.4 Pyroresistance from Phytic Acid

Pyroresistance is defined here as the behaviour of a material when exposed to heat and flames. Thermogravimetric analysis (TGA) observes a materials thermal stability as it degrades due to heat, while cone calorimetry determines the flammability. In Paper I and II, cellulose fibers in the form of filters and foams were treated with PA. The effects of heat treatment and phosphorus on thermal stability were evaluated in Paper I, while a comparison to cross-linked citric acid and the effects of foam additives were analyzed in Paper II.

Organophosphates such as PA act as fire-retardant materials due to their ability to form a char layer in the condensed phase, and mitigate radical reactions in the gas phase. At the onset of carbonization T_{onset}, PA decomposes quickly via pyrolysis to form phosphoric acids. Similarly to the cross-linking mechanisms described in Section 4.1, phosphates catalyze the dehydration of cellulose and form a char layer. This char layer is a carbonaceous glass layer that forms on the surface of the condensed phase, shielding the material below from heat and oxygen.[73,78,162] This transition is marked by the presence of a shoulder at 250-300 °C in TGA (Figure 4.12a,b).

Increases in T_{onset} were directly correlated with a decrease in phosphorus content due to the washing out or degradation of non-cross-linked phosphates (Figures 4.2d and 4.12b). The reduced phosphorus content of P160 could be attributed to the thermal decomposition of PA at 150-160 °C.[119] This observation between T_{onset} and phosphorus content was consistent with reports in other studies at higher concentrations of PA.[113,117,124,163–166] However, the degree of change in T_{onset} with respect to heat treatment, and thus phosphorus content, and was inconsistent. The act of cross-linking phosphates to cellulose further increased carbonization temperature as covalent ester bonds blocked the depolymerization of cellulose.

As the char layer formed, there was a simultaneous steep loss in mass as material decomposed during pyrolysis. Phosphorylated cellulose resulted in faster carbonization rates (C_{rate}), which promoted rapid formation of the char layer. This layer led to lower weight loss and the start of the degradation plateau at lower temperatures. The quality and speed of char layer formation were therefore critical to the thermo-oxidative stability from 300-500 °C. In cellulose fiber foams, PA also extended the plateau to higher combustion temperatures (T_{max2}). This was attributed to the strong interaction between

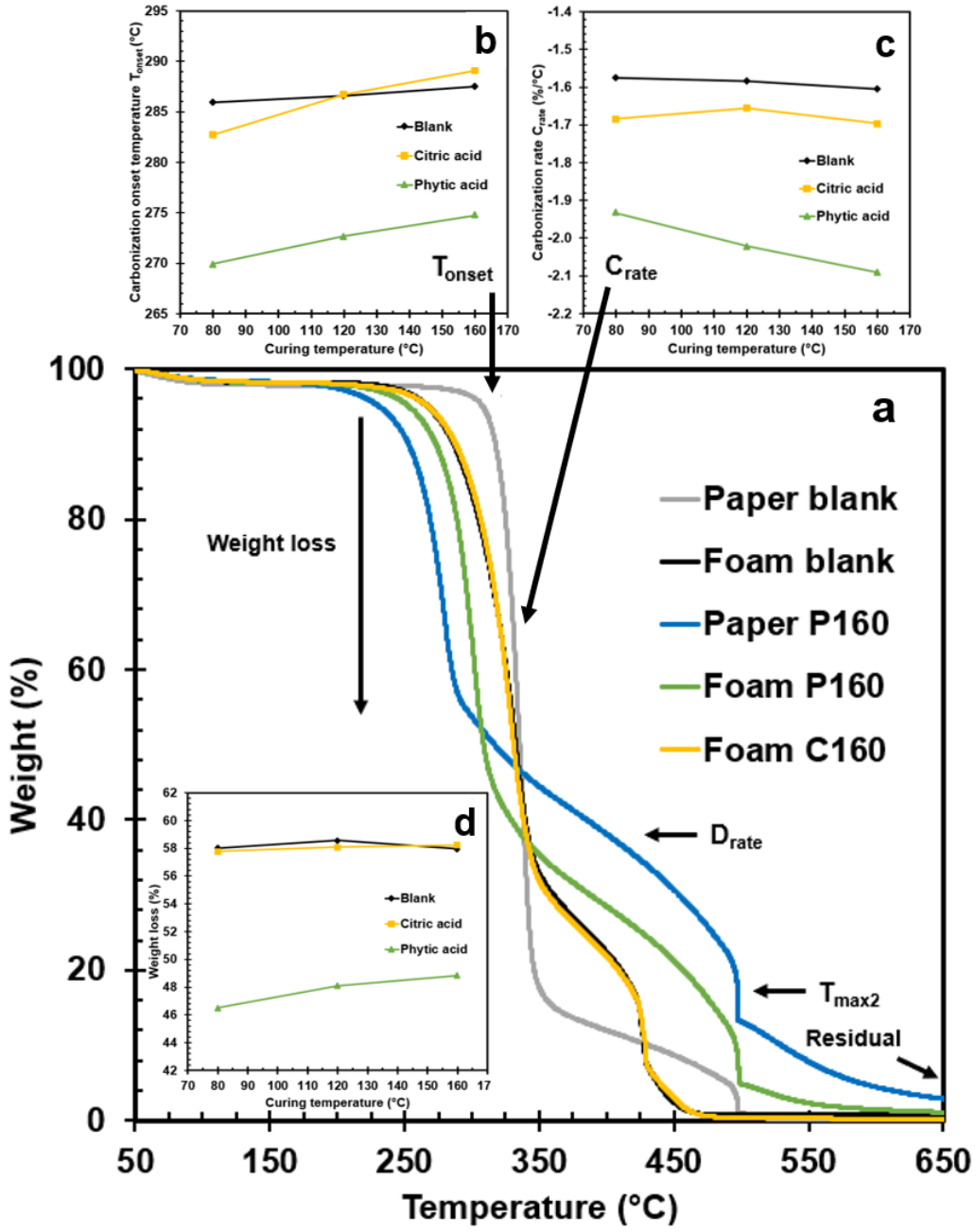

Figure 4.12: TGA thermo-oxidative stability a) full temperature range curves with effects of cross-linking on b) carbonization onset temperature, c) carbonization rate, and d) weight loss. Reproduced from Orzan et al. under Creative Commons CC-BY license.[111,125]

PA and CMC, which prevented early combustion of CMC at 380 °C.[167,168] Overall, phosphorylating cellulose led to improved thermo-oxidative stability at temperatures above 300 °C.

Cone calorimetry expanded on TGA analysis by unveiling how the cross-linking of PA to cellulose affected the fire-retardant performance of the foams (Table 4.3). PA foams exhibited a lower time to ignition (TTI), resulting in fast charring. In addition, the peak and total heat release rate (PHRR, THR) were significantly lower than the blank and citric acid cross-linked foams. This slowed the fire growth rate (FGR) as pyrolysis in the condensed phase and combustion in the gas phase were reduced. The layer also prevented the release of volatile particles from combustion, reducing the total smoke production (TSP). In comparison, CA cross-linking had no significant effect on blank foams in TGA. The CA foams did slow fire growth rate, but also increased heat release and smoke production. PA cellulose fiber foams could be considered self-extinguishing and reached a Euroclass E classification, which is the minimum for insulation materials in building codes (EN 13501).[112]

Table 4.3: Cone calorimetry analysis of cellulose fiber foams for: time to ignition (TTI), peak heat release rate (PHRR), total heat release (THR), fire growth rate (FGR) and total smoke production (TSP). Reproduced from Orzan et al. under Creative Commons CC-BY license.[125]

Foam	TTI (s)	PHRR (kW/m^2)	THR (MJ/m^2)	FGR ($kJ/m^2/s$)	TSP (m^2)
80	9.3	118	20	9.1	0.11
120	9.3	117	20	9.0	0.23
160	4.7	119	18	9.2	0.14
P80	8.3	99	19	7.6	0.03
P120	4.7	85	18	4.0	0.06
P160	3.3	86	17	4.5	0.05
C80	9.7	133	22	8.3	0.13
C120	9.7	124	22	6.9	0.22
C160	8.3	116	21	5.5	0.19

CHAPTER 5

Concluding Remarks and Outlook

This thesis focused on the modification of cellulose and foam formation to create strengthened fiber foams. Two distinct methods for creating solid foams from cellulose were evaluated: i) cross-linking using phytic acid or xylan, and ii) morphological restructuring using tert-butanol in cryogels. In each, the interactions of additives with cellulose and how they influence foaming behaviour provides the context of foam development in the wet-state. Using differing drying methods, unique pore structuring and fiber network configurations produced solid foams with varying mechanical properties and additional functionalities.

In the first approach, phytic acid was employed as a new multi-functional cross-linker. Where typically this compound was used for fire-retardant textiles, this study also sought to explore its value in cellulose fiber foams. Phytic acid changed the foaming behaviour of systems containing an ionic surfactant, SDS, and viscosifier, CMC. Binding interactions between CMC and phytic acid led to improved foamability due to viscous effects encapsulating gas bubbles

and reducing drainage and coarsening. However, the drop in pH decreased electrostatic repulsion and disjoining pressure, leading to rapid collapse of the wet foams.

Another side effect of phytic acid was its degradation of cellulose fibers via partial hydrolysis. This became evident in ^{13}C NMR as cellulose crystallinity increased, and solid foams displayed poor mechanical strength in compression. An important question was raised: Could covalent cross-linking between fibers overcome the mechanical deterioration resulting from degradation? To evaluate this, catalyst-free dehydration synthesis reactions were used to form di-ester cross-links between phytic acid and cellulose at different heat treatment temperatures. With heat treatment temperatures of 160 °C, phytic acid cross-linked cellulose fiber foams managed to outperform blank foams and could be considered a competitive alternative to a popular cross-linker, citric acid. The foams displayed unique mechanical behaviours, providing a new degree of freedom when tailoring cellulose fiber foams towards particular applications. The additional thermal stability and fire-retardancy provided by the char layer formation of phytic acid undermines the inherent weakness of cellulose to fire.

The studies with phytic acid underlined the value of inter-fiber cross-linking over intrinsic cellulosic structures for reinforcing fiber foam networks. In a separate approach, native xylan hemicelluloses were either adsorbed to or enzymatically degraded from cellulose fibers. The trend was clear: an increase in xylan content led to improved mechanical properties, credit to a denser network that enabled fiber-fiber bonding. However, the relative value of intrinsic xylan compared to adsorbed extrinsic xylan could not be understated. A loss of just 1 wt% intrinsic xylan was more impactful on properties than a 3 wt% extrinsic adsorption. This could be pointed to the aggregated form of xylans on the surface of fibers failing to act as sufficient reinforcement.

Use of covalent or physical cross-linking methods led to similar trends of improved modulus and strength in fiber networks. Energy absorption had a minimal increase, yet was strongly affected by both enzymatic and phytic acid fiber degradation. These findings suggest that the preservation of intrinsic cellulose structures is paramount when considering applications which require strength and impact absorption. Therefore, pulping processes and products should be considered carefully when selecting cellulose fibers. In contrast, the initial elastic response and stiffness of fiber networks benefits more from cross-linking with less detriment from degradation.

The structural organization of CNCs within foams represents the second approach to strengthening. Where other studies focus on using TBA to increase surface area, here we exploited its crystal formation to produce mechanically sound pore structures. Upon freezing, the effect of TBA-water interactions on crystal formation created cryogels with unique morphological features. At 30-50 wt% TBA, the strength of the CNC network was maximized, owing to the change from lamellar sheets to a netted/capillary structure. The eutectic mixture of TBA and water at 20 and 90 wt% TBA instead developed mesoporosity, maximizing surface area. This study showcased how co-solvents can be used to modulate properties in foams. The addition of over 30 wt% TBA disrupted the ordered anisotropic assembly of CNC suspensions. TBA adsorbed to hydrophobic CNC interfaces and lowered the Debye length, causing network percolation and increased viscoelastic properties. This method required the use of a solvent but led to the most pronounced change in mechanical properties and no changes in mass compared to the proposed cross-linking methods. Further study on the effect of network percolation inside cryogel pore walls on mechanical and thermal properties would give fascinating insights into the roles of fibrillar structures and pore morphology.

The methods underlined in this thesis are by no means comprehensive. The diversity of research surrounding both cellulose and foams leaves a promising note for the future of these materials. And while cellulose is a good prospective choice to replace plastics, a plethora of other bio-based materials such as alginates, chitosan, pectins and starch may provide valuable solution. In terms of strengthening fiber networks of cellulose, work is necessary to understand the value of each intrinsic component and structure in fibers. This would allow pulp manufacturers to produce fibers efficiently for a wider variety of applications. It also encourages cross-linking methods via cellulose regeneration to be mindful of how to reconstruct polysaccharide networks. Cellulose fiber networks also struggle with producing highly elastic products unaffected by moisture. Solutions in both pore structuring and fiber composition are needed to overcome these challenges. The final hurdle which limits the use of cellulose and other bio-based materials in solid foams is drying. The time and energy input needed to remove water places considerable limitations on the viability of industrial-scale production.

References

[1] Marc André Meyers et al. "Biological materials: Structure and mechanical properties". In: *Progress in materials science* 53.1 (2008), pp. 1–206.

[2] Yasuaki Seki, Matthew S Schneider, and Marc A Meyers. "Structure and mechanical behavior of a toucan beak". In: *Acta Materialia* 53.20 (2005), pp. 5281–5296.

[3] Marc André Meyers and Po-Yu Chen. *Biological Materials Science: Biological materials, Bioinspired materials and biomaterials*. London, UK: Cambridge University Press, 2014.

[4] Yasuaki Seki, Sara G Bodde, and Marc A Meyers. "Toucan and hornbill beaks: a comparative study". In: *Acta Biomaterialia* 6.2 (2010), pp. 331–343.

[5] Yves Bienvenu. "Application and future of solid foams". In: *Comptes Rendus Physique* 15.8 (2014). Liquid and solid foams / Mousses liquides et solides, pp. 719–730. ISSN: 1631-0705.

[6] James Njuguna. *Lightweight Composite Structures in Transport: Design, Manufacturing, Analysis and Performance*. Woodhead Publishing, 2016.

[7] Tony R Walker and Lexi Fequet. "Current trends of unsustainable plastic production and micro (nano) plastic pollution". In: *TrAC Trends in Analytical Chemistry* 160 (2023), p. 116984.

[8] Eliott Orzan. "Upgrading Cellulose Networks: Conquering Limitations in Fiber Foams". In: *Licentiate Thesis* (2023).

[9] Lorna J. Gibson and Michael F. Ashby. *Cellular Solids: Structure and Properties*. 2nd ed. Cambridge Solid State Science Series. Cambridge University Press, 1997.

[10] J. J. Bikerman. *Foams*. Springer-Verlag, New York, 1973.

[11] Cosimo Brondi et al. "Role of air bubble inclusion on polyurethane reaction kinetics". In: *Materials* 15.9 (2022), p. 3135.

[12] Nurbol Tolganbek et al. "Design and preparation of thin film gel polymer electrolyte for 3D Li-ion battery". In: *Journal of Power Sources* 493 (2021), p. 229686.

[13] M.F. Ashby. *Materials Selection in Mechanical Design*. Pergamon Press, 1992.

[14] Petronela Nechita and Silviu Marian Năstac. "Overview on foam forming cellulose materials for cushioning packaging applications". In: *Polymers* 14.10 (2022), p. 1963.

[15] Omar Faruk, Andrzej K Bledzki, and Laurent M Matuana. "Microcellular foamed wood-plastic composites by different processes: A review". In: *Macromolecular Materials and Engineering* 292.2 (2007), pp. 113–127.

[16] Denis L Weaire and Stefan Hutzler. *The Physics of Foams*. Oxford University Press, 1999.

[17] Gilbert D Miles and John Ross. "Foam Stability of Solutions of Soaps of Pure Fatty Acids." In: *The Journal of Physical Chemistry* 48.5 (1944), pp. 280–290.

[18] Kathirvel Ganesan et al. "Design of aerogels, cryogels and xerogels of cellulose with hierarchical porous structures". In: *Materials & Design* 92 (2016), pp. 345–355.

[19] Kathirvel Ganesan et al. "Influence of hierarchical porous structures on the mechanical properties of cellulose aerogels". In: *Journal of Sol-Gel Science and Technology* 89 (2019), pp. 156–165.

[20] Henrik Bäckdahl et al. “Engineering microporosity in bacterial cellulose scaffolds”. In: *Journal of Tissue Engineering and Regenerative Medicine* 2.6 (2008), pp. 320–330.

[21] Nicole Pircher et al. “Preparation and reinforcement of dual-porous biocompatible cellulose scaffolds for tissue engineering”. In: *Macromolecular Materials and Engineering* 300.9 (2015), pp. 911–924.

[22] D Fennell Evans and Håkan Wennerström. *The Colloidal Domain: Where Physics, Chemistry, Biology, and Technology Meet*. Wiley-Vch, New York, 1999.

[23] Wei Yu and Mazen Y Kanj. “Review of foam stability in porous media: The effect of coarsening”. In: *Journal of Petroleum Science and Engineering* 208 (2022), p. 109698.

[24] Jianlong Wang, Anh V Nguyen, and Saeed Farrokhpay. “A critical review of the growth, drainage and collapse of foams”. In: *Advances in Colloid and Interface science* 228 (2016), pp. 55–70.

[25] Timo Lappalainen and Jani Lehmonen. “Paper physics: determinations of bubble size distribution of foam-fibre mixture using circular hough transform”. In: *Nordic Pulp & Paper Research Journal* 27.5 (2012), pp. 930–939.

[26] Arnaud Saint-Jalmes. “Physical chemistry in foam drainage and coarsening”. In: *Soft Matter* 2.10 (2006), pp. 836–849.

[27] A Madani et al. “Ultra-lightweight paper foams: processing and properties”. In: *Cellulose* 21 (2014), pp. 2023–2031.

[28] Ran Li et al. “Ultra-lightweight cellulose foam material: preparation and properties”. In: *Cellulose* 24 (2017), pp. 1417–1426.

[29] Tuomo Hjelt et al. “Foam forming of fiber products: A review”. In: *Journal of Dispersion Science and Technology* 43.10 (2022), pp. 1462–1497.

[30] Pouyan Jahangiri et al. “On filtration and heat insulation properties of foam formed cellulose based materials”. In: *Nordic Pulp & Paper Research Journal* 29.4 (2014), pp. 584–591.

[31] Samuel Stephens Kistler. “Coherent expanded aerogels and jellies”. In: *Nature* 127.3211 (1931), pp. 741–741.

[32] Nathalie Lavoine and Lennart Bergström. “Nanocellulose-based foams and aerogels: processing, properties, and applications”. In: *Journal of Materials Chemistry A* 5.31 (2017), pp. 16105–16117.

[33] Elisa S Ferreira, Camila A Rezende, and Emily D Cranston. "Fundamentals of cellulose lightweight materials: bio-based assemblies with tailored properties". In: *Green Chemistry* 23.10 (2021), pp. 3542–3568.

[34] Thomas Metzger et al. "Understanding and preventing structural changes during drying of gels". In: *Modern Drying Technology* (2011).

[35] Peter Kubbutat, Luísa Leitão, and Ulrich Kulozik. "Stability of foams in vacuum drying processes. Effects of interactions between sugars, proteins, and surfactants on foam stability and dried foam properties". In: *Foods* 10.8 (2021), p. 1876.

[36] Anita Etale et al. "Cellulose: a review of water interactions, applications in composites, and water treatment". In: *Chemical reviews* 123.5 (2023), pp. 2016–2048.

[37] Alvaro Tejado et al. "Superhydrophobic foam-like cellulose made of hydrophobized cellulose fibres". In: *Cellulose* 21 (2014), pp. 1735–1743.

[38] Aleksandra Borisova et al. "A sustainable freeze-drying route to porous polysaccharides with tailored hierarchical meso-and macroporosity". In: *Macromolecular Rapid Communications* 36.8 (2015), pp. 774–779.

[39] Nela Buchtová and Tatiana Budtova. "Cellulose aero-, cryo-and xerogels: Towards understanding of morphology control". In: *Cellulose* 23 (2016), pp. 2585–2595.

[40] Oona Korhonen and Tatiana Budtova. "All-cellulose composite aerogels and cryogels". In: *Composites Part A: Applied Science and Manufacturing* 137 (2020), p. 106027.

[41] Guang Chu et al. "Ice-assisted assembly of liquid crystalline cellulose nanocrystals for preparing anisotropic aerogels with ordered structures". In: *Chemistry of Materials* 29.9 (2017), pp. 3980–3988.

[42] Severine Vessot and Julien Andrieu. "A review on freeze drying of drugs with tert-butanol (TBA)+ water systems: characteristics, advantages, drawbacks". In: *Drying Technology* 30.4 (2012), pp. 377–385.

[43] Dirk L Teagarden and David S Baker. "Practical aspects of lyophilization using non-aqueous co-solvent systems". In: *European Journal of Pharmaceutical Sciences* 15.2 (2002), pp. 115–133.

[44] Miran Mavlan et al. "Mechanochemical esterification of cellulose nanofibers lyophilized from eutectic water–tert-butanol mixtures". In: *Cellulose* 30.14 (2023), pp. 8805–8817.

[45] J Bevan Ott, J Rex Goates, and Boyd A Waite. "(Solid+ liquid) phase equilibria and solid-hydrate formation in water+ methyl,+ ethyl,+ isopropyl, and+ tertiary butyl alcohols". In: *The Journal of Chemical Thermodynamics* 11.8 (1979), pp. 739–746.

[46] Bakul S Bhatnagar et al. "A refined phase diagram of the tert-butanol–water system and implications on lyophilization process optimization of pharmaceuticals". In: *Physical Chemistry Chemical Physics* 22.3 (2020), pp. 1583–1590.

[47] Kasra Kasraian and Patrick P DeLuca. "Thermal analysis of the tertiary butyl alcohol-water system and its implications on freeze-drying". In: *Pharmaceutical Research* 12 (1995), pp. 484–490.

[48] Rim Daoussi et al. "Freeze-drying of an active principle ingredient using organic co-solvent formulations: influence of freezing conditions and formulation on solvent crystals morphology, thermodynamics data, and sublimation kinetics". In: *Drying Technology* 29.16 (2011), pp. 1858–1867.

[49] Thomas Buchecker et al. "The impact of the structuring of hydrotropes in water on the mesoscale solubilisation of a third hydrophobic component". In: *Physical Chemistry Chemical Physics* 19.3 (2017), pp. 1806–1816.

[50] Hao Jin et al. "Nanofibrillar cellulose aerogels". In: *Colloids and Surfaces A: Physicochemical and Engineering Aspects* 240.1-3 (2004), pp. 63–67.

[51] Samir U Sane and Chung C Hsu. "Considerations for successful lyophilization process scale-up, technology transfer, and routine production". In: *Formulation and process development strategies for manufacturing biopharmaceuticals*. John Wiley & Sons Inc Hoboken, NJ, 2010, p. 797.

[52] Arun S Mujumdar and Evangelos Tsotsas. *Modern drying technology*. Wiley-VCH, 2007.

[53] Arun S Mujumdar. "Superheated steam drying". In: *Handbook of industrial drying* 2 (1995), pp. 1071–1086.

[54] Rachna Sehrawat, Prabhat K Nema, and Barjinder Pal Kaur. "Effect of superheated steam drying on properties of foodstuffs and kinetic modeling". In: *Innovative Food Science & Emerging Technologies* 34 (2016), pp. 285–301.

[55] C Pronyk, S Cenkowski, and WE Muir. "Drying foodstuffs with superheated steam". In: *Drying Technology* 22.5 (2004), pp. 899–916.

[56] Tariq Aziz et al. "A Review on the Modification of Cellulose and Its Applications". In: *Polymers* 14.15 (2022). ISSN: 2073-4360.

[57] AD French et al. "Encyclopedia of polymer science and technology". In: *Cellulose* 1838 (2018).

[58] Dieter Klemm et al. "Cellulose: fascinating biopolymer and sustainable raw material". In: *Angewandte Chemie International Edition* 44.22 (2005), pp. 3358–3393.

[59] Alain Dufresne. "Nanocellulose: a new ageless bionanomaterial". In: *Materials Today* 16.6 (2013), pp. 220–227.

[60] Daniel J Cosgrove. "Growth of the plant cell wall". In: *Nature reviews molecular cell biology* 6.11 (2005), pp. 850–861.

[61] Ingo Burgert. "Exploring the micromechanical design of plant cell walls". In: *American Journal of Botany* 93.10 (2006), pp. 1391–1401.

[62] H Sixta et al. *Handbook of Pulp*. Wiley-VHC Verlag GmbH and Co., 2006.

[63] RE Kirk. *Kirk-Othmer Encyclopedia of Chemical Technology.(Vol. 16)*. Wiley, New York, 1991.

[64] Marc Delgado Aguilar et al. "Approaching a low-cost production of cellulose nanofibers for papermaking applications". In: *Bioresources* 10.3 (2015), pp. 5435–5355.

[65] Camilla Abbati de Assis et al. "Conversion economics of forest biomaterials: risk and financial analysis of CNC manufacturing". In: *Biofuels, Bioproducts and Biorefining* 11.4 (2017), pp. 682–700.

[66] Gwendoline Delepierre et al. "Benchmarking cellulose nanocrystals Part II: New industrially produced materials". In: *Langmuir* 37.28 (2021), pp. 8393–8409.

[67] Tomas Rosén et al. "Cross-sections of nanocellulose from wood analyzed by quantized polydispersity of elementary microfibrils". In: *ACS nano* 14.12 (2020), pp. 16743–16754.

[68] Camilla Abbati de Assis et al. "Cellulose micro-and nanofibrils (CMNF) manufacturing-financial and risk assessment". In: *Biofuels, Bioproducts and Biorefining* 12.2 (2018), pp. 251–264.

[69] Ana Paula Marinho Bloot et al. "A review of phytic acid sources, obtention, and applications". In: *Food Reviews International* 39.1 (2023), pp. 73–92.

[70] Lei Wang et al. “Isolation and characteristics of nanocellulose from hardwood pulp via phytic acid pretreatment”. In: *Industrial Crops and Products* 182 (2022), p. 114921.

[71] Kusmono and MN Affan. “Isolation and characterization of nanocrystalline cellulose from ramie fibers via phosphoric acid hydrolysis”. In: *Journal of Natural Fibers* 19.7 (2022), pp. 2744–2755.

[72] Quanquan Guo et al. “Biological phytic acid as a multifunctional curing agent for elastomers: towards skin-touchable and flame retardant electronic sensors”. In: *Green Chemistry* 19.14 (2017), pp. 3418–3427.

[73] Wei Liu et al. “A bio-based flame retardant coating used for polyamide 66 fabric”. In: *Progress in Organic Coatings* 156 (2021), p. 106271.

[74] Xiao-hui Liu et al. “Durable flame retardant cellulosic fibers modified with novel, facile and efficient phytic acid-based finishing agent”. In: *Cellulose* 25 (2018), pp. 799–811.

[75] Fei Song et al. “Biobased coating derived from fish scale protein and phytic acid for flame-retardant cotton fabrics”. In: *Materials & Design* 221 (2022), p. 110925.

[76] Xian-Ting Zheng et al. “Fully bio-based flame-retardant cotton fabrics via layer-by-layer self assembly of laccase and phytic acid”. In: *Journal of Cleaner Production* 350 (2022), p. 131525.

[77] A Richard Horrocks and Dennis Price. *Fire retardant materials*. Woodhead Publishing, 2001.

[78] Karin Aschberger et al. “Chemical alternatives assessment of different flame retardants–A case study including multi-walled carbon nanotubes as synergist”. In: *Environment International* 101 (2017), pp. 27–45.

[79] Sammaiah Thota et al. “Covalent functionalization of cellulose in cotton and a nylon-cotton blend with phytic acid for flame retardant properties”. In: *Cellulose* 27 (2020), pp. 11–24.

[80] Hua-Bin Yuan, Ren-Cheng Tang, and Cheng-Bing Yu. “Flame Retardant functionalization of microcrystalline cellulose by phosphorylation reaction with phytic acid”. In: *International Journal of Molecular Sciences* 22.17 (2021), p. 9631.

[81] Zhisen Wang et al. “Cellulose nanocrystal/phytic acid reinforced conductive hydrogels for antifreezing and antibacterial wearable sensors”. In: *Carbohydrate Polymers* 298 (2022), p. 120128.

[82] Charles Q Yang, Xilie Wang, and In-Sook Kang. "Ester crosslinking of cotton fabric by polymeric carboxylic acids and citric acid". In: *Textile Research Journal* 67.5 (1997), pp. 334–342.

[83] Zijing Cai et al. "Investigation on reaction sequence and group site of citric acid with cellulose characterized by FTIR in combination with two-dimensional correlation spectroscopy". In: *Polymers* 11.12 (2019), p. 2071.

[84] Elisa S Ferreira, Emily D Cranston, and Camila A Rezende. "Naturally hydrophobic foams from lignocellulosic fibers prepared by ovendrying". In: *ACS Sustainable Chemistry & Engineering* 8.22 (2020), pp. 8267–8278.

[85] A Meftahi et al. "Preventing the collapse of 3D bacterial cellulose network via citric acid". In: *Journal of Nanostructure in Chemistry* 8 (2018), pp. 311–320.

[86] Anna Ottenhall, Tiinamari Seppänen, and Monica Ek. "Water-stable cellulose fiber foam with antimicrobial properties for bio based low-density materials". In: *Cellulose* 25.4 (2018), pp. 2599–2613.

[87] Adriana Nicoleta Frone et al. "Bacterial cellulose sponges obtained with green cross-linkers for tissue engineering". In: *Materials Science and Engineering: C* 110 (2020), p. 110740.

[88] Jukka A Ketoja et al. "Compression strength mechanisms of low-density fibrous materials". In: *Materials* 12.3 (2019), p. 384.

[89] Tero Mäkinen et al. "Crossover from mean-field compression to collective phenomena in low-density foam-formed fiber material". In: *Soft Matter* 16.29 (2020), pp. 6819–6825.

[90] Tiina Pöhler et al. "On the strength improvement of lightweight fibre networks by polymers, fibrils and fines". In: *Cellulose* 27 (2020), pp. 6961–6976.

[91] Per Bergström, Shakhawath Hossain, and Tetsu Uesaka. "Scaling behaviour of strength of 3D-, semi-flexible-, cross-linked fibre network". In: *International Journal of Solids and Structures* 166 (2019), pp. 68–74.

[92] Sara Paunonen et al. "Improving compression recovery of foam-formed fiber materials". In: *BioResources* 13.2 (2018), pp. 4058–4074.

[93] Nela Buchtová et al. "Mechanical properties of cellulose aerogels and cryogels". In: *Soft Matter* 15 (39 2019), pp. 7901–7908.

[94] Markus Wagner et al. “Pulp fibre foams: Morphology and mechanical performance”. In: *Composites Part A: Applied Science and Manufacturing* 188 (2025), p. 108515. ISSN: 1359-835X.

[95] Romain Sescousse, Roxane Gavillon, and Tatiana Budtova. “Aerocellulose from cellulose–ionic liquid solutions: preparation, properties and comparison with cellulose–NaOH and cellulose–NMMO routes”. In: *Carbohydrate Polymers* 83.4 (2011), pp. 1766–1774.

[96] Tiina Pöhler et al. “Use of papermaking pulps in foam-formed thermal insulation materials”. In: *Nordic Pulp & Paper Research Journal* 32.3 (2017), pp. 367–374.

[97] P Nechita and S Năstac. “Foam-formed cellulose composite materials with potential applications in sound insulation”. In: *Journal of Composite Materials* 52.6 (2018), pp. 747–754.

[98] Andreja Dobaj Štiglic et al. “Organic acid cross-linked 3D printed cellulose nanocomposite bioscaffolds with controlled porosity, mechanical strength, and biocompatibility”. In: *IScience* 25.5 (2022).

[99] Isabel Mira et al. “Foam forming revisited Part I. Foaming behaviour of fibre-surfactant systems”. In: *Nordic Pulp & Paper Research Journal* 29.4 (2014), pp. 679–688.

[100] Annika E Ketola et al. “Changing the structural and mechanical anisotropy of foam-formed cellulose materials by affecting bubble–fiber interaction with surfactant”. In: *ACS Applied Polymer Materials* 4.10 (2022), pp. 7685–7698.

[101] Christian Demitri et al. “Novel superabsorbent cellulose-based hydrogels crosslinked with citric acid”. In: *Journal of Applied Polymer Science* 110.4 (2008), pp. 2453–2460.

[102] Matthew J Baker et al. “Using Fourier transform IR spectroscopy to analyze biological materials”. In: *Nature Protocols* 9.8 (2014), pp. 1771–1791.

[103] Bernd Reif et al. “Solid-state NMR spectroscopy”. In: *Nature Reviews Methods Primers* 1.1 (2021), p. 2.

[104] Gerhard Zuckerstätter et al. “The elucidation of cellulose supramolecular structure by 13C CP-MAS NMR”. In: *Lenzinger Berichte* 87.January (2009), pp. 38–46.

[105] Cy M Jeffries et al. “Small-angle X-ray and neutron scattering”. In: *Nature Reviews Methods Primers* 1.1 (2021), p. 70.

[106] Olof Theander and Eric A Westerlund. "Studies on dietary fiber. 3. Improved procedures for analysis of dietary fiber". In: *Journal of Agricultural and Food Chemistry* 34.2 (1986), pp. 330–336.

[107] Joanna Wojtasz-Mucha, Merima Hasani, and Hans Theliander. "Hydrothermal pretreatment of wood by mild steam explosion and hot water extraction". In: *Bioresource Technology* 241 (2017), pp. 120–126.

[108] Stephen Brunauer, Paul Hugh Emmett, and Edward Teller. "Adsorption of gases in multimolecular layers". In: *Journal of the American Chemical Society* 60.2 (1938), pp. 309–319.

[109] Fleur Rol et al. "Cellulose phosphorylation comparison and analysis of phosphorate position on cellulose fibers". In: *Carbohydrate Polymers* 229 (2020), p. 115294.

[110] Vanja Kokol et al. "Characterisation and properties of homo-and heterogenously phosphorylated nanocellulose". In: *Carbohydrate Polymers* 125 (2015), pp. 301–313.

[111] Eliott Orzan et al. "Elucidation of cellulose phosphorylation with phytic acid". In: *Industrial Crops and Products* 218 (2024), p. 118858.

[112] Karina Antoun et al. "Renewable phosphorous-based flame retardant for lignocellulosic fibers". In: *Industrial Crops and Products* 186 (2022), p. 115265.

[113] Marco Barbalini et al. "Hybrid silica-phytic acid coatings: Effect on the thermal stability and flame retardancy of cotton". In: *Polymers* 11.10 (2019), p. 1664.

[114] Xian-Wei Cheng et al. "Preparation and evaluation of an eco-friendly, reactive, and phytic acid-based flame retardant for wool". In: *Reactive and Functional Polymers* 134 (2019), pp. 58–66.

[115] Jian Liu et al. "Eco-friendly flame retardant and smoke suppression coating containing boron compounds and phytic acids for nylon/cotton blend fabrics". In: *Industrial Crops and Products* 186 (2022), p. 115239.

[116] Xuqin Xie et al. "Phytic acid-based hybrid complexes for improving the interfacial property and mildew-resistance of heat-treated bamboo". In: *Colloids and Surfaces A: Physicochemical and Engineering Aspects* 659 (2023), p. 130749.

[117] Maryam Ghanadpour et al. "Phosphorylated cellulose nanofibrils: a renewable nanomaterial for the preparation of intrinsically flame-retardant materials". In: *Biomacromolecules* 16.10 (2015), pp. 3399–3410.

[118] Flynn T Watson, Ronald J Smernik, and Ashlea L Doolette. "Thermal degradation of phytate produces all four possible inositol pentakisphosphates as determined by ion chromatography and 1H and 31P NMR spectroscopy". In: *Phosphorus, Sulfur, and Silicon and the Related Elements* 194.12 (2019), pp. 1140–1148.

[119] André Luis Máximo Daneluti and Jivaldo do Rosário Matos. "Study of thermal behavior of phytic acid". In: *Brazilian Journal of Pharmaceutical Sciences* 49 (2013), pp. 275–283.

[120] Roger H Newman. "Carbon-13 NMR evidence for cocrystallization of cellulose as a mechanism for hornification of bleached kraft pulp". In: *Cellulose* 11 (2004), pp. 45–52.

[121] Kristina Wickholm, Per Tomas Larsson, and Tommy Iversen. "Assignment of non-crystalline forms in cellulose I by CP/MAS 13C NMR spectroscopy". In: *Carbohydrate Research* 312.3 (1998), pp. 123–129.

[122] Jin-Chao Zhang, Chao-Jun Wu, and Dong-Mei Yu. "Effect of phosphoric acid in the prehydrolysis process of dissolving pulp production from bamboo-willow". In: *BioResources* 14.2 (2019), pp. 3117–3131.

[123] Jinbao Li et al. "Foam materials with controllable pore structure prepared from nanofibrillated cellulose with addition of alcohols". In: *Industrial Crops and Products* 125 (2018), pp. 314–322.

[124] Yanan Ma et al. "Eco-friendly, efficient and durable fireproof cotton fabric prepared by a feasible phytic acid grafting route". In: *Cellulose* 28 (2021), pp. 3887–3899.

[125] E Orzan et al. "Foaming and cross-linking of cellulose fibers using phytic acid". In: *Carbohydrate Polymers* 347 (2025), p. 122617.

[126] Alina Ghilan et al. "One-Step Preparation of Carboxymethyl Cellulose—Phytic Acid Hydrogels with Potential for Biomedical Applications". In: *Gels* 8.10 (2022), p. 647.

[127] Alexandar Metodiev Zhivkov. "Electric properties of carboxymethyl cellulose". In: *Cellulose–Fundamental Aspects*. Ed. by Theo van de Ven and Louis Godbout. Rijeka, Croatia: IntechOpen, 2013. Chap. 8.

[128] AA Moosavi-Movahedi et al. "A distinct intermediate of RNase A is induced by sodium dodecyl sulfate at its pKa". In: *Colloids and Surfaces B: Biointerfaces* 43.3-4 (2005), pp. 150–157.

[129] Jure Cerar et al. “Structural, rheological and dynamic aspects of hydrogen-bonding molecular liquids: Aqueous solutions of hydrotropic tert-butyl alcohol”. In: *Journal of Colloid and Interface Science* 560 (2020), pp. 730–742.

[130] Michael D Hands and Lyudmila V Slipchenko. “Intermolecular interactions in complex liquids: effective fragment potential investigation of water–tert-butanol mixtures”. In: *The Journal of Physical Chemistry B* 116.9 (2012), pp. 2775–2786.

[131] M Kiselev and D Ivlev. “The study of hydrophobicity in water–methanol and water–tert-butanol mixtures”. In: *Journal of Molecular Liquids* 110.1-3 (2004), pp. 193–199.

[132] DT Bowron, AK Soper, and JL Finney. “Temperature dependence of the structure of a 0.06 mole fraction tertiary butanol-water solution”. In: *The Journal of Chemical Physics* 114.14 (2001), pp. 6203–6219.

[133] Paschalis Alexandridis, Ulf Olsson, and Björn Lindman. “A record nine different phases (four cubic, two hexagonal, and one lamellar lyotropic liquid crystalline and two micellar solutions) in a ternary isothermal system of an amphiphilic block copolymer and selective solvents (water and oil)”. In: *Langmuir* 14.10 (1998), pp. 2627–2638.

[134] Neta Cohen et al. “Polymer-induced modification of cellulose nanocrystal assemblies in aqueous suspensions”. In: *ACS Applied Polymer Materials* 2.2 (2019), pp. 732–740.

[135] Pierre Munier et al. “Assembly of cellulose nanocrystals and clay nanoplatelets studied by time-resolved X-ray scattering”. In: *Soft Matter* 17.23 (2021), pp. 5747–5755.

[136] Kazuki Furukawa, Satoshi Shibuta, and Ken Judai. “Viscosity study of tert-butyl alcohol aqueous solution by Brownian motion and gravimetric capillaries”. In: *Journal of Molecular Liquids* 319 (2020), p. 114170.

[137] Julien Schmitt et al. “Surfactant induced gelation of TEMPO-oxidized cellulose nanofibril dispersions probed using small angle neutron scattering”. In: *The Journal of Chemical Physics* 158.3 (2023), p. 034901.

[138] Ashok C Kumbharkhane, Sanjay M Puranik, and Suresh C Mehrotra. “Dielectric relaxation of tert-butyl alcohol–water mixtures using a time-domain technique”. In: *Journal of the Chemical Society, Faraday Transactions* 87.10 (1991), pp. 1569–1573.

[139] U Kaatze, A Schumacher, and R Pottel. "The dielectric properties of tert.-butanol/water mixtures as a function of composition". In: *Berichte der Bunsengesellschaft für Physikalische Chemie* 95.5 (1991), pp. 585–592.

[140] Bruno Medronho et al. "Rationalizing cellulose (in) solubility: reviewing basic physicochemical aspects and role of hydrophobic interactions". In: *Cellulose* 19 (2012), pp. 581–587.

[141] Yoichi Kanda, Shin Iwasaki, and Ko Higashitani. "Adhesive force between hydrophilic surfaces in alcohol–water solutions". In: *Journal of Colloid and Interface Science* 216.2 (1999), pp. 394–400.

[142] Somia Haouache et al. "Edge-On (Cellulose II) and Face-On (Cellulose I) Adsorption of Cellulose Nanocrystals at the Oil–Water Interface: A Combined Entropic and Enthalpic Process". In: *Biomacromolecules* 23.9 (2022), pp. 3517–3524.

[143] Saina Kishani et al. "Entropy drives the adsorption of xyloglucan to cellulose surfaces–a molecular dynamics study". In: *Journal of Colloid and Interface Science* 588 (2021), pp. 485–493.

[144] Charles Bruel et al. "The structural amphiphilicity of cellulose nanocrystals characterized from their cohesion parameters". In: *Carbohydrate Polymers* 205 (2019), pp. 184–191.

[145] Richard M Parker et al. "The self-assembly of cellulose nanocrystals: Hierarchical design of visual appearance". In: *Advanced Materials* 30.19 (2018), p. 1704477.

[146] NA Seaton. "Determination of the connectivity of porous solids from nitrogen sorption measurements". In: *Chemical Engineering Science* 46.8 (1991), pp. 1895–1909.

[147] Matthieu Fumagalli et al. "Gas-phase esterification of cellulose nanocrystal aerogels for colloidal dispersion in apolar solvents". In: *Soft Matter* 9.47 (2013), pp. 11309–11317.

[148] Maria-Ximena Ruiz-Caldas et al. "Anisotropic foams derived from textile-based cellulose nanocrystals and xanthan gum". In: *Carbohydrate Polymers* 338 (2024), p. 122212.

[149] Clémentine Darpentigny et al. "Ice-templated freeze-dried cryogels from tunicate cellulose nanocrystals with high specific surface area and anisotropic morphological and mechanical properties". In: *Cellulose* 27 (2020), pp. 233–247.

[150] Daniel A Osorio et al. "Morphology of cross-linked cellulose nanocrystal aerogels: cryo-templating versus pressurized gas expansion processing". In: *Journal of Materials Science* 53 (2018), pp. 9842–9860.

[151] Xuan Yang and Emily D Cranston. "Chemically cross-linked cellulose nanocrystal aerogels with shape recovery and superabsorbent properties". In: *Chemistry of Materials* 26.20 (2014), pp. 6016–6025.

[152] Houssine Sehaqui, Qi Zhou, and Lars A. Berglund. "High-porosity aerogels of high specific surface area prepared from nanofibrillated cellulose (NFC)". In: *Composites Science and Technology* 71.13 (2011), pp. 1593–1599. ISSN: 02663538.

[153] Junji Nemoto, Tsuguyuki Saito, and Akira Isogai. "Simple freeze-drying procedure for producing nanocellulose aerogel-containing, high-performance air filters". In: *ACS Applied Materials & Interfaces* 7.35 (2015), pp. 19809–19815.

[154] Anurodh Tripathi et al. "Expanding the upper limits of robustness of cellulose nanocrystal aerogels: outstanding mechanical performance and associated pore compression response of chiral-nematic architectures". In: *Journal of Materials Chemistry A* 7.25 (2019), pp. 15309–15319.

[155] Åsa Henriksson and Paul Gatenholm. "Controlled assembly of glucuronoxylans onto cellulose fibres". In: *Holzforschung* (2001).

[156] Åsa Linder et al. "Mechanism of assembly of xylan onto cellulose surfaces". In: *Langmuir* 19.12 (2003), pp. 5072–5077.

[157] Mirza Faisal Qaseem and Ai-Min Wu. "Balanced xylan acetylation is the key regulator of plant growth and development, and cell wall structure and for industrial utilization". In: *International Journal of Molecular Sciences* 21.21 (2020), p. 7875.

[158] Janne Laine, R Hynynen, and P Stenius. "The effect of surface chemical composition and charge on the fibre and paper properties of unbleached and bleached kraft pulps". In: *Fundamental Research Symposium: The Fundamentals of Papermaking Materials*. Pira International. 1997, pp. 859–892.

[159] Christa Schönberg et al. "The importance of xylan for the strength properties of spruce kraft pulp fibres". In: *Holzforschung* 55.6 (2001).

[160] John Sjöberg et al. "Fiber surface composition and its relations to papermaking properties of soda-anthraquinone and kraft pulps". In: *Nordic Pulp & Paper Research Journal* 19.3 (2004), pp. 392–396.

[161] Veronika Biegler et al. “Effect of xylan on the mechanical performance of softwood kraft pulp 2D papers and 3D foams”. In: *TAPPI JOURNAL* 24.3 (2025), pp. 131–141.

[162] Bernhard Schartel. “Phosphorus-based flame retardancy mechanisms—old hat or a starting point for future development?” In: *Materials* 3.10 (2010), pp. 4710–4745.

[163] Xian-Wei Cheng et al. “Covalent flame-retardant functionalization of wool fabric using ammonium phytate with improved washing durability”. In: *Industrial Crops and Products* 187 (2022), p. 115332.

[164] Yajuan Feng et al. “A plant-based reactive ammonium phytate for use as a flame-retardant for cotton fabric”. In: *Carbohydrate Polymers* 175 (2017), pp. 636–644.

[165] Gaopeng Jiang, Jinli Qiao, and Feng Hong. “Application of phosphoric acid and phytic acid-doped bacterial cellulose as novel proton-conducting membranes to PEMFC”. In: *International Journal of Hydrogen Energy* 37.11 (2012), pp. 9182–9192.

[166] Ling Sun et al. “Preparation, characterization and testing of flame retardant cotton cellulose material: flame retardancy, thermal stability and flame-retardant mechanism”. In: *Cellulose* 28 (2021), pp. 3789–3805.

[167] S El-Sayed et al. “DSC, TGA and dielectric properties of carboxymethyl cellulose/polyvinyl alcohol blends”. In: *Physica B: Condensed Matter* 406.21 (2011), pp. 4068–4076.

[168] Sahar I Mostafa et al. “Adsorption and interaction studies of methylene blue dye onto agar-carboxymethylcellulose-silver nanocomposite in aqueous media”. In: *Biomass Conversion and Biorefinery* 14.3 (2024), pp. 3363–3383.